

Response to Associate Editor Comments
(G. Gehrels, 28 May, 2020)

(Blue = AE comment; black = response to comment; red = changes to manuscript)

I'll start this review-response with a general explanation that my approach to presenting and interpreting geochronologic data is very different from the AE's.

My approach is to determine the dates and uncertainties of zircon crystals as accurately as possible, and then propagate the dates and the measured uncertainties through every aspect of data presentation and interpretation. Including the uncertainties is essential given that they vary considerably as a function of age, U conc, common Pb content, matrix variations, etc.

The approach advocated by the AE is to ignore the measured analytical uncertainties in data presentation and interpretation. Instead, researchers are encouraged to portray age distributions data using KDE's, which utilize uncertainties that are specified by the user (by adjusting the bandwidth). These KDE's (based on measured dates and user-specified uncertainties) are then used for all descriptions and interpretations.

This approach is advocated in the review recommendation which states:

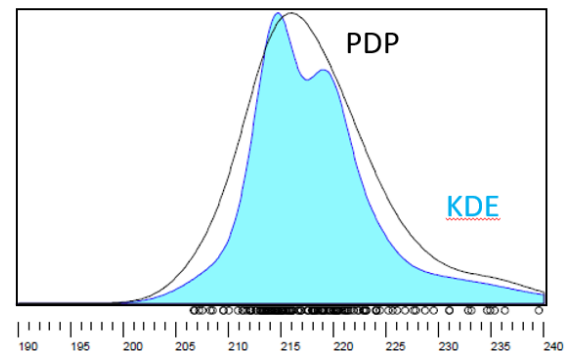
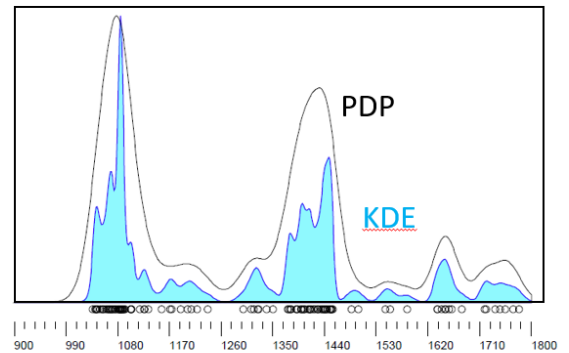
"Furthermore, if you replace your Probability Density Plots (PDPs) by Kernel Density Estimates (KDEs), then you can tweak their bandwidth to produce the most informative result."

I would argue that this approach is fundamentally flawed for two reasons:

First is the observation that KDE's generate inaccurate and misleading age distributions. This is demonstrated on the accompanying plot, which compares PDP and KDE curves for sample 182. The curves were generated utilizing the density plotter (v. 8.5) routine from Vermeesch (2012), assuming the bandwidth generated by the routine (3.12). Primary issues are as follows:

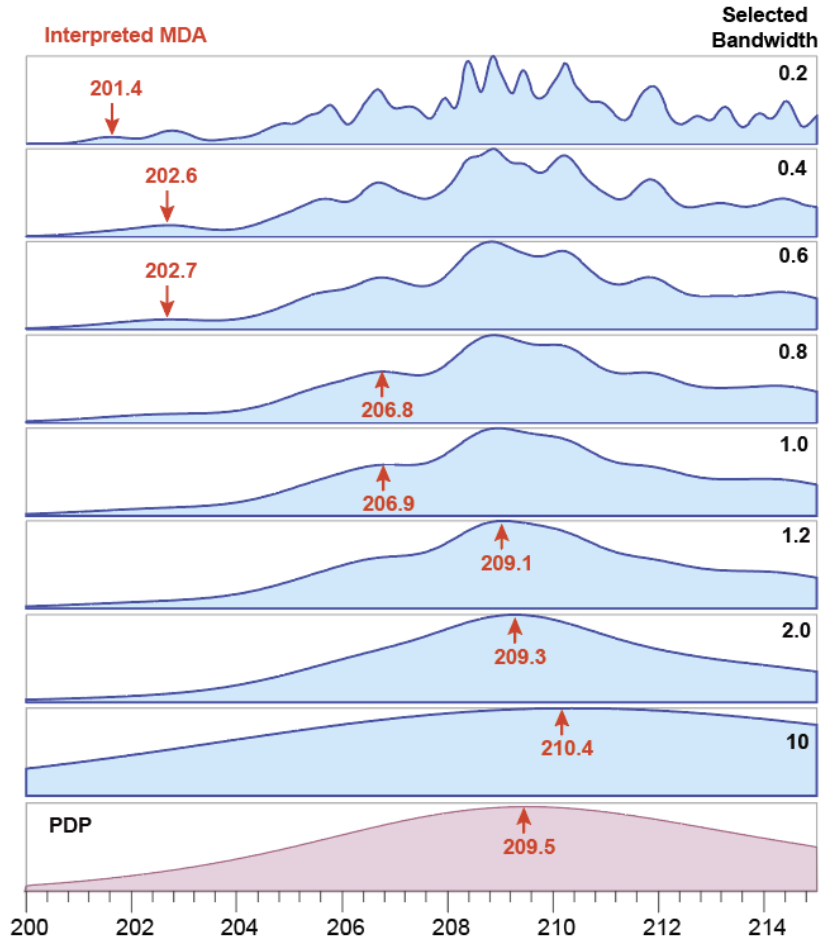
-- The default KDE bandwidth forces uncertainties of the individual analyses to be reduced to ~ 0.4 of their measured values. Standard analyses demonstrate that there is no basis for these lower uncertainties.

-- For provenance analysis, the upper plot shows that KDE curves contain many more age peaks than the PDP. There is no observational basis for the additional age peaks -- they are simply an artifact of assuming lower uncertainties.



-- For max depo age analysis, the lower curve shows that the KDE has two age peaks (~214.6 and ~219.1 Ma), whereas the PDP curve contains only one peak (~216.0 Ma). There is no observational basis for shifting of the younger peak age, or recognition of two distinct age groups -- both result simply from the incorrect assumption of lower uncertainties.

Second, providing a researcher with the capability to "tweak their bandwidth to produce the most informative result" is hugely problematic. The accompanying plot shows how selection of different bandwidths impacts the age of the youngest cluster of dates for sample 52. The lower (pink) curve shows the PDP for all dates and measured uncertainties, which yields a peak age of 209.5 Ma. The upper blue curves show KDE's for the same data, now utilizing various bandwidths. Peak ages for the youngest clusters on these KDE's range from 210.4 to 201.4, based entirely on the subjective choice of bandwidth.



Given these issues, I conclude that it is not appropriate to use KDE's to describe the data presented in this paper. KDE calculations are based on uncertainties that clearly are incorrect, and the resulting KDE age distributions are inaccurate and prone to subjective bias. Given that the KDE age distributions are incorrect, it is also inappropriate to use them for interpretive aspects of the analysis, for example MDS comparison of age distributions.

Specific responses to the AE comments are inserted below.

Sharman Review:

1. Dr. Sharman gave a positive review that raises one major point and several minor ones. The major concern was about the lack of evidence to support the inference that near depositional

age zircon is air-fall in origin and older zircon is recycled. You responded to this comment by saying that you are:

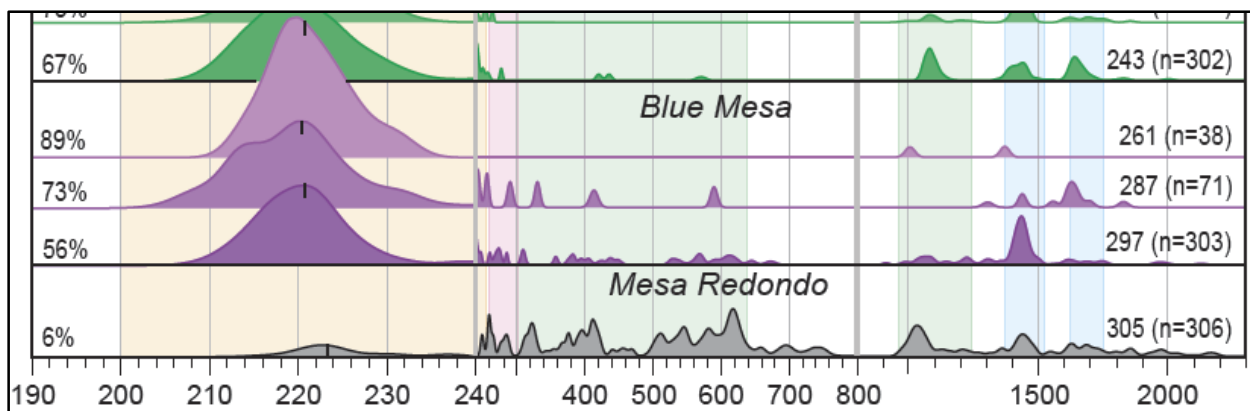
unable to provide reliable information about morphology of the young grains, as most were plucked out from the mounts and dissolved for CA-TIMS geochronology. We tried to do this analysis with BSE images of the grains (before analysis), but the size/shape of the grains in the images has little bearing on the true size/shape of the grains. This because the mounts were polished down just a little so as to retain more material for the CA-TIMS analyses.

I would have thought that even a two-dimensional cross section through a c-axis parallel zircon grain would reveal whether the grain is prismatic or not. If you have stored the BSE images, then I would encourage you to include them in an online data repository.

Response: As noted in the manuscript and response to Sharman's review, the BSE images do not provide sufficient information to determine the size/shape of grains analyzed. This is because the images show only a very small portion of the grain that was exposed during a light polishing. The size/shape of this exposed area has no bearing on the true size/shape of the grain, and so would be highly misleading.

2. The reviewer also has a question about the change in scale of your age distributions. An alternative way to bump the height of the pre-240Ma age component would be to plot the age distributions on a logarithmic time scale. Furthermore, if you replace your Probability Density Plots (PDPs) by Kernel Density Estimates (KDEs), then you can tweak their bandwidth to produce the most informative result. As you know, cumulative distributions are also useful for data visualization. They, too, can be plotted on a logarithmic time axis.

Response: Indeed there are many alternatives to the present PDP plots. But KDE plots are highly misleading (as described above), and none of the other options (e.g., log scale or cumulative plots) would provide the essential information as clearly as the current plots (a portion of which is shown below).



Ramezani Review:

1. Stratigraphy: Dr Ramezani is concerned that the observed drift between your MDAs and the depositional ages is due to misidentification of the stratigraphic positions in the CPCP core. In your response, you wrote that your paper does not aim to present an age model, and does not claim to estimate accurate MDAs either. I am a bit confused, because the paper does seem to me like an attempt to calibrate the depositional history of the CPCP core in absolute time. If your paper has a different objective, then please state more clearly what the purpose of the study actually is. I apologise if I am missing something obvious here.

Response:

It's not clear why the AE assumes that the purpose of the paper is to present an age model. Many different sections clarify the purpose of the paper, and provide a connection with age models:

1. The title does not indicate any attempt to determine an age model:

" LA-ICPMS U-Pb geochronology of detrital zircon grains from the Coconino, Moenkopi, and Chinle Formations in the Petrified Forest National Park (Arizona)"

2. The introduction clearly states the purpose of the paper, with no mention of constructing an age model (p. 82-85 of the revised draft):

"This report explores variations in both provenance and maximum depositional age of strata intersected in the CPCP-PFNP13-1A core, and the implications for Permian-Triassic environmental and biotic transformations and the tectonic evolution of southwestern North America."

3. Our discussion of the use of MDA's clearly states that age models referred to in the paper are from previous work (lines 571-575):

"As part the Colorado Plateau Coring Project, Kent et al. (2018) and Rasmussen et al. (2020) report the results of CA-TIMS analyses on many of the same samples reported herein. All of the available CA-TIMS ages, and the preferred age models of Kent et al. (2019) and Rasmussen et al. (2020), are shown on Figure 13."

4. Connection of our data with age models published in previous studies is clearly stated on lines 673-677:

"Figure 13 presents a comparison of our preferred maximum depositional ages, all available ID- and CA-TIMS ages [from Riggs et al. (2003), Heckert et al. (2009), Ramezani et al. (2011), Irmis et al. (2011), Atchley et al. (2013), Nordt et al., (2015), Kent et al. (2018), and Rasmussen et al.

(2019)], and two age models that are based on magnetostratigraphic and CA-TIMS geochronologic information (Kent et al., 2019; Rasmussen et al., 2019)."

And on lines 877-882:

"4. Comparison of the Chinle Formation MDA's with magnetostratigraphic information (Kent et al., 2018, 2019) and CA-TIMS geochronologic information (Rasmussen et al., 2019) from the CPCP core, plus CA-TIMS ages reported from outcrop samples, indicates that LA-ICPMS MDA's approximate depositional ages for most strata of the Mesa Redondo Member, Blue Mesa Member, and Petrified Forest Member, but significantly pre-date deposition for strata of the Sonsela Member (Fig. 13).

2. U-Pb geochronology: Dr. Ramenazi is concerned that the LA-ICP-MS results may be affected by Pb-loss, which would invalidate their use as maximum depositional ages. In your response, you write that:

This manuscript goes to great length to document that Pb loss is a significant factor for many of the grains analyzed. We show this internally with the Uconce tests described above. We also document this by comparison of our ages with the CA-TIMS data from the same grains (Appendix 2). Indeed, Pb loss is an important factor for many of our analyses! But the assertion that LA-ICPMS max depo ages are younger than the CA-TIMS ages of Ramezani et al. (2011) and Atchley et al. (2013) due to Pb loss is not supported by the fact that most of the reported LA-ICPMS MDA's are older (not younger) than the equivalent MDA's reported by R+2011 and A+ 2013!!

Appendix 2 clearly shows that the LA-ICP-MS data are consistently 5-10 Ma younger than the CA-TIMS ages. To me this confirms the reviewer's concerns. The fact that the ad-hoc MDA estimates for the youngest LA-ICP-MS peak (which are shown as circles in Appendix 2) are consistently older than the CA-TIMS estimates (which are shown as red bars in Appendix 2) is a result of comparing datasets of different size. Your LA-ICP-MS based MDA estimate uses more grains than the CA-TIMS estimate, making the comparison between the two estimates biased. This problem is diagnostic of a fundamental flaw in three of the four MDA estimation algorithms that are proposed in the manuscript. I will discuss this in more detail below.

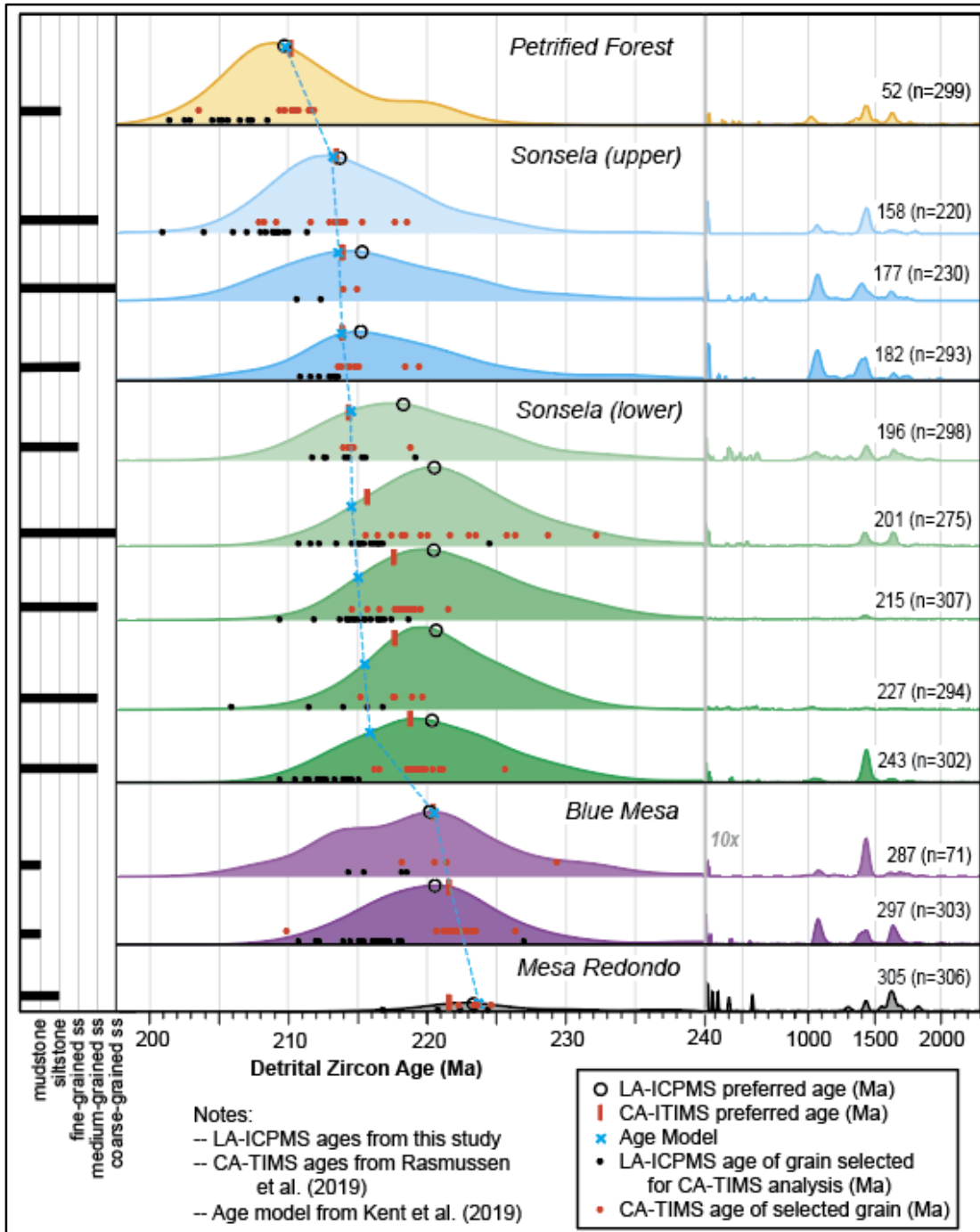
Response: There are two/three different issues embedded in this comment.

The first concerns whether the LA-ICPMS MDAs are older or younger than the CA-TIMS MDAs. I'm so glad the AE brought attention to this issue, as it turns out that the symbols (circles and red bars) were reversed on the original version of Appendix 2! No wonder Ramezani went off on a tirade about Pb loss!

The revised version is inserted below, and it shows that, for the twelve samples with both LA-ICPMS MDAs and CA-TIMS MDAs:

- no samples yield LA-ICPMS MDAs that are significantly younger than the CA-TIMS MDAs
- no samples yield LA-ICPMS MDAs that are significantly younger than the age models.
- LA-ICPMS MDAs are indistinguishable from CA-TIMS MDAs and age models for five samples
- LA-ICPMS MDAs are older than the CA-TIMS MDAs and age models for seven samples

➔ The fact that not a single one of our MDAs is younger than the age models provides strong evidence that Pb loss has not compromised our MDAs, and that our method for determining the MDAs is reliable.



→ A revised version of Appendix 2 has been prepared.

It is not clear whether the statement "the LA-ICP-MS data are consistently 5-10 Ma younger than the CA-TIMS ages" is related to the mis-labeling issue noted above, or is related to the individual LA-ICPMS vs CA-TIMS dates (red/black dots in this figure). If the latter, a reasonable explanation is presented in the manuscript: These grains have indeed lost Pb -- that's why they're on the young side of the age distribution, and that's why the CA-TIMS dates for these grains are older. But the fact that none of the LA-ICPMS MDAs are younger than the CA-TIMS MDAs, or the model ages, suggests that the LA-ICPMS MDAs are not compromised by Pb loss. That's just what the data show!

The second/third issue has to do with the process used to determine the MDA's from our LA-ICPMS data. As noted above, the strategy pursued in this manuscript is to use community accepted methods to characterize the age of a set of dates and associated uncertainties. And to do this in a way that makes the fewest possible assumptions about which dates to include or exclude. The original version of the manuscript described some of the issues with the methods, mostly having to do with the need to include/exclude analyses from the calculations. In response to the AE comment, we have added the following statement (lines 234-241):

"Complications with these methods arise from (1) the need to make unconstrained decisions about which analyses to include or exclude from consideration, (2) the evidence from complicated PDP age distributions and high (>1.0) MSWD values that the youngest clusters for most samples contain multiple age populations, (3) the evidence that dates in some clusters have been compromised by Pb loss, and (4) issues of statistical robustness for some methods (Vermeesch, 2018b)."

In spite of these issues, we retain the conclusion that a combination of the results from the four methods yield impressively accurate average MDAs for many of our samples. Given that none of the 23 reported MDA's are younger than the CA-TIMS ages or the age model, there simply is no evidence to support the AE concern that our MDA's are too young due to issues with the statistical methods.

Further Comments:

1. The paper uses four different heuristic MDA estimation algorithms. Three of these methods are problematic, because they drift to ever younger ages with increasing sample size.

(a) Age of the youngest peak on a probability density plot (PDP): PDPs have no statistical basis, and any quantitative information derived from them is of dubious statistical significance. If you were to analyse one million grains of zircon, then the youngest age cluster on a PDP would likely be younger than the actual depositional age.

Response: Agreed, PDP has no statistical basis. It is simply the algebraic sum of the measured dates and uncertainties. There is no evidence in this data set that the PDP peak age is younger

than the depositional age -- in fact 22 of 23 PDP peak ages are the same age or older than the age model determined by magnetostrat and CA-TIMS ages.

(b) Weighted Mean age and uncertainty of the youngest cluster: Same problem. Any heuristic method that is based on p-values is problematic because p-values are a sensitive function of sample size. The larger the sample size, the greater the likelihood that the χ^2 -test identifies spurious peaks.

Response: Same as above, this is a community accepted method for determining the mean age of a set of dates. There is no evidence the weighted mean ages are younger than the depositional age -- in fact all 23 weighted mean ages are the same age (within uncertainty) or older than the age model determined by magnetostrat and CA-TIMS ages.

(c) Maximum Likelihood age and uncertainty. See Figure 6.3 of Vermeesch (2018b) for an example of how multimodal unmixing models suffer from the same problem as methods a. and b.

Response: Same as above -- it's a community accepted method that yields reliable results for this data set. All 23 "unmix" ages are the same age (within uncertainty) or older than the age model determined by magnetostrat and CA-TIMS ages.

The sample size dependency is actually reported in the paper ("Ironically, the more grains analyzed, the greater the inaccuracy of [the] youngest age!"). I do not understand why these broken methods are still used in the paper and would advocate that they are removed. In statistics, it is desirable for estimates to asymptotically converge to the truth with increasing sample size. Only the Tuffzirc age model may have this property. An alternative would be the parametric minimum age model of Galbraith and Laslett (1993). But neither of these techniques is immune to the Pb-loss problem.

Response: This comment provides strong support that the PDP, unmix, and weighted mean MDA's are not biased, as all three methods yield results that are similar to the Tuffzirc MDA's. As shown in DR Table 6, for the 31 samples that yield results for all four metrics, the Tuffzirc age is the oldest for only two -- it is the youngest for seven and in the middle for the other twenty-two. There accordingly is no evidence to support the view that the other methods yield MDA's that are two young.

To represent the AE's concerns about the statistical validity of these methods, we have noted in the Analytical Methods section that issues with these methods are noted by Vermeesch (2018b).

2. The paper frequently uses two ad-hoc dissimilarity measures called 'Likeness' and 'Cross-correlation Coefficient' (CCC). These quantities are both derived from PDPs and are flawed for reasons that are given in detail by Vermeesch (2018a). Please remove these from the paper and replace them with bona fide statistical dissimilarity measures such as the Kolmogorov-Smirnov

statistic. Of course, if you can present a statistically valid argument against my objections to Likeness and CCC, then I would be happy to change my mind.

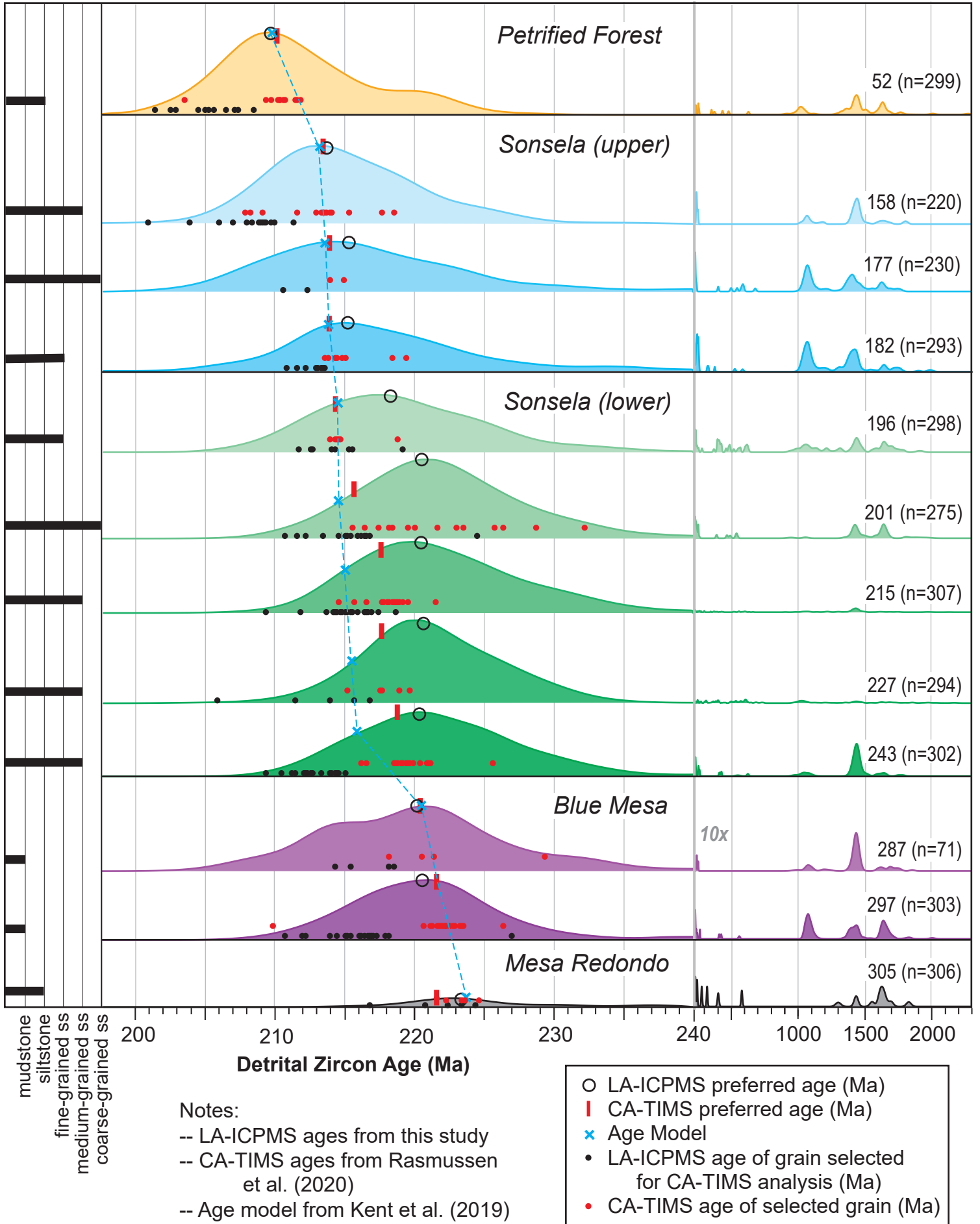
Likeness, Similarity, and Cross-correlation coefficient methods have been reported by Gehrels (2000), Sundell and Saylor (2016), Wissink et al. (2018), and Sharman et al. (2018), and are widely used and accepted by the geochronologic community. The robustness of these methods is demonstrated by the fact that they yield very similar results as the K-S statistic favored by the AE. Detailed results of all four methods are presented in DR Table 4 so that readers can compare the results for themselves.

We have also noted in the Analytical Methods section that issues with some of these methods have been raised by Vermeesch (2018a).

3. Is Figure 10 a two-dimensional PDP or KDE? I think that this diagram would be more effective as a contour plot, or as a simple scatter plot. The three-dimensional effect adds no useful information.

Response: These are based on KDEs because uncertainties of the two variables are not important. With regard to the 3-d effect, I think this helps readers evaluate similarities/differences of the various units.

Appendix 2 (CA-TIMS vs LA-ICPMS ages)



24 **ABSTRACT**

25 U-Pb geochronology was conducted by Laser Ablation-Inductively Coupled Plasma Mass
26 Spectrometry (LA-ICPMS) on [7,175](#) detrital zircon grains from twenty-nine samples from the
27 Coconino Sandstone, Moenkopi Formation, and Chinle Formation. These samples were
28 recovered from ~520 m of drill core that was acquired during the Colorado Plateau Coring
29 Project (CPCP), located in Petrified Forest National Park (Arizona).

30 A sample from the lower Permian Coconino Sandstone yields a broad distribution of
31 Proterozoic and Paleozoic ages that are consistent with derivation from the Appalachian and
32 Ouachita orogens, with little input from local basement or Ancestral Rocky Mountain sources.
33 Four samples from the Holbrook Member of the Moenkopi Formation yield a different set of
34 Precambrian and Paleozoic age groups, indicating derivation from the Ouachita orogen, the
35 East Mexico Arc, and the Permo-Triassic arc built along the Cordilleran margin.

36 Twenty-three samples from the Chinle Formation contain variable proportions of Proterozoic
37 and Paleozoic zircon grains, but are dominated by Late Triassic grains. LA-ICPMS ages of these
38 grains belong to five main groups that correspond to the Mesa Redondo Member, Blue Mesa
39 Member and lower part of the Sonsela Member, upper part of the Sonsela Member, middle
40 part of the Petrified Forest Member, and upper part of the Petrified Forest Member. The ages
41 of pre-Triassic grains also correspond to these chronostratigraphic units, and are interpreted to
42 reflect varying contributions from the Appalachian orogen to the east, Ouachita orogen to the
43 southeast, Precambrian basement exposed in the Ancestral Mogollon Highlands to the south,
44 East Mexico arc, and Permian-Triassic arc built along the southern Cordilleran margin. Triassic
45 grains in each chronostratigraphic unit also have distinct U and Th concentrations, which are
46 interpreted to reflect temporal changes in the chemistry of arc magmatism.

47 Comparison of our LA-ICPMS ages with available CA-TIMS ages and new magnetostratigraphic
48 data provides new insights into the depositional history of the Chinle Formation, as well as
49 methods utilized to determine depositional ages of fluvial strata. For parts of the Chinle
50 Formation that are dominated by fine-grained clastic strata (e.g. mudstone and siltstone), such
51 as the Blue Mesa Member and Petrified Forest Member, all three chronometers agree (to
52 within ~1 m.y.), and robust depositional chronologies have been determined. In contrast, for
53 stratigraphic intervals dominated by coarse-grained clastic strata (e.g., sandstone), such as
54 most of the Sonsela Member, the three chronologic records disagree due to recycling of older
55 zircon grains and variable dilution of syn-depositional-age grains. This results in LA-ICPMS ages
56 that significantly pre-date deposition, and CA-TIMS ages that range between the other two
57 chronometers. These complications challenge attempts to establish a well-defined
58 chronostratigraphic age model for the Chinle Formation, ~~and to evaluate possible connections~~
59 ~~among fundamental Late Triassic biotic and climatic changes and a red siliceous horizon~~
60 ~~encountered in the CPCP core.~~

61 1. INTRODUCTION

62 Triassic strata of the Colorado Plateau and environs provide rich and geographically extensive
63 records of environmental and biotic change during a critical period of Earth history, as well as
64 the transition from passive- to convergent-margin tectonism along the North American
65 Cordillera (e.g., Parker and Martz, 2011; Olsen et al., 2011). As demonstrated by Riggs et al.
66 (1996, 2003, 2012, 2013, 2016), Dickinson and Gehrels (2008), Irmis et al. (2011), Ramezani et
67 al. (2011, 2014), Atchley et al. (2013), Nordt et al. (2015), Kent et al. (2018, 2019), Olsen et al.
68 (2018, 2019), Marsh et al. (2019), and Rasmussen et al. (202019), Chinle Formation strata have
69 the potential to record the timing of these changes in great detail given their several-hundred-
70 meter thickness, abundance of near-depositional-age zircon grains, and recoverable
71 paleomagnetic reversal stratigraphy.

72 In an effort to further develop this record, ~520 m of continuous core was collected from
73 Triassic and underlying Permian strata at Petrified Forest National Park (PEFO), which is located
74 on the southern Colorado Plateau of northern Arizona (Fig. 1; [\(35.085933° N, 109.795500° W,](#)
75 [WGS84 datum\)](#)). The objectives and primary findings of this project have been described by
76 Olsen et al. (2018, 2019), Kent et al. (2018, 2019), and Rasmussen et al. (202019), and
77 numerous related studies are currently in progress. This contribution to the project reports ~~on~~
78 U-Pb geochronologic analyses of detrital zircon grains that were extracted from twenty-nine
79 samples from this core (CPCP-PFNP13-1A). Analyses were conducted by laser ablation-
80 inductively coupled mass spectrometry (LA-ICPMS), with between 36 and 490 grains analyzed
81 per sample [\(total of 7,175 analyses\)](#). Grains were chosen for analysis by random selection in an
82 effort to provide unbiased information about provenance. Fortunately, a significant number of
83 near-depositional-age grains were recovered from many samples in the Chinle Formation,
84 which provides opportunities to also determine robust maximum depositional ages. This report
85 explores variations in both provenance and maximum depositional age of strata intersected in
86 the CPCP-PFNP13-1A core, and the implications for Permian-Triassic environmental and biotic
87 transformations and the tectonic evolution of southwestern North America.

88 2. STRATA ENCOUNTERED IN THE PETRIFIED FOREST NATIONAL PARK DRILL CORE

89 The lowest stratigraphic horizon encountered consists of quartz arenite belonging to the
90 Coconino Sandstone (Fig. 2). This unit belongs to regionally extensive erg deposits of early
91 Permian (Leonardian) age (Blakey et al., 1988; Lawton et al., 2015; Dickinson, 2018).

92 Overlying strata of the Coconino Sandstone are tabular, thin to thick-bedded, reddish
93 mudstone, siltstone, and sandstone layers of the Lower-Middle Triassic Moenkopi Formation. In
94 the PEFO region, the Moenkopi Formation consists of thin-bedded reddish siltstone with
95 interlayered sandstone and mudstone. Lower, finer-grained strata are assigned to the Wupatki
96 Member and Moqui Member, and upper sandstone-rich horizons dominate the Holbrook
97 Member. The base is a regional unconformity, the TR-1 unconformity of Pipiringos and
98 O'Sullivan (1978), along which strata of the lower Permian Toroweap Formation and Kaibab

99 Formation have been removed. Strata of the Moenkopi Formation are interpreted to have
100 accumulated on a northwest-sloping coastal plain, with thinner fluvial strata to the southeast
101 and thicker marginal marine strata to the northwest (Dickinson, 2018). The Moenkopi
102 Formation basin was bounded by residual uplifts of the Ancestral Rocky Mountains to the
103 northeast and highlands of the Ouachita orogen to the southeast. Highlands developed within
104 early phases of the Cordilleran magmatic arc may have existed to the southwest.

105 Strata of the Moenkopi Formation are overlain unconformably [Tr-3 unconformity of Pippingos
106 and O'Sullivan (1978)] by the Chinle Formation (Fig. 2). The transition is marked in most areas
107 by the Shinarump Conglomerate, which consists of cobbles of chert, quartzite, limestone and
108 subordinate felsic volcanic rocks. Riggs et al. (2012) have determined U-Pb ages of 232-224 Ma
109 on volcanic cobbles in the Shinarump Conglomerate. The Shinarump Conglomerate is
110 interpreted to correlate with finer-grained strata of the Mesa Redondo Member (Irmis et al.,
111 2011; Martz et al., 2012, 2017; Riggs et al., 2016). Strata of the Shinarump Conglomerate and
112 Mesa Redondo Member are interpreted to have accumulated in paleovalleys that were carved
113 into underlying strata. Strikingly variegated, strongly pedogenically modified, red, purple, and
114 yellow strata in the core are assigned to the Mesa Redondo Member given the lack of
115 conglomerate. Strata of the Mesa Redondo Member in outcrop have yielded U-Pb (~~zircon~~
116 ages of ~227.6 Ma (Atchley et al., 2013) and ~225.2 Ma (Ramezani et al., 2011).

117 Gradationally overlying the Mesa Redondo Member are strata of the Blue Mesa Member,
118 which consist of purplish to gray and red bentonitic mudstone with sandstone beds that are
119 generally 0.5 m in thickness (Woody, 2006). Blue Mesa Member mudstones are pervasively
120 pedogenically modified in the core. These strata are interpreted to have accumulated primarily
121 as overbank deposits within a mixed-load meandering river system (Martz and Parker, 2010).
122 Previously reported U-Pb (ID-TIMS or CA-TIMS) ages from outcrop of the Blue Mesa Member
123 range from ~223 Ma to ~218 Ma (Heckert et al., 2009; Ramezani et al., 2011; Irmis et al., 2011;
124 Atchley et al., 2013; Rasmussen et al., 2020~~19~~).

125 Strata of the Blue Mesa Member are overlain by sandstone-rich and conglomerate-bearing
126 strata of the Sonsela Member. Lucas (1993) and Heckert and Lucas (2002) refer to the base of
127 the Sonsela Member as a regionally significant unconformity, although this interpretation has
128 been questioned by Woody (2006) and Martz and Parker (2010) given that conglomeratic
129 sandstone of the Sonsela is interbedded with mudstone of the Blue Mesa Member. Martz and
130 Parker (2010) suggest that the transition from the Blue Mesa Member to the Sonsela Member
131 marks a change in depositional regime (from mainly overbank deposits to bedload-dominated
132 channel deposits) but does not mark a significant hiatus in deposition.

133 The Sonsela Member consists predominantly of sandstone with lesser mudstone and local
134 conglomerate. Sandstone beds are variable in thickness, have significant lateral extent, and
135 exhibit cut-and-fill structure (Woody, 2006). Conglomerate (with abundant volcanic clasts) is
136 common within the sandstone beds. Five units have been recognized, a lower sandstone
137 interval (Camp Butte beds), a lower-middle unit with abundant mudstone (Lot's Wife beds), a

138 middle sandstone and conglomerate unit (Jasper Forest/Rainbow Forest bed), a middle-upper
139 unit with pedogenic carbonate and abundant mudstone (Jim Camp Wash beds), and an upper
140 sandstone unit (Martha's Butte beds) (Martz and Parker, 2010). The five units are gradational,
141 with the main variation being the abundance of mudstone in two of the middle units. A reddish
142 siliceous horizon of uncertain regional extent has been recognized within the middle of the
143 upper mudstone-rich unit in the CPCP-PFNP13-1A core. Similar horizons within other exposures
144 of the Sonsela Member are marked by a significant die-off of the conifers that characterize
145 Petrified Forest National Park (Creber and Ash, 1990), a turn-over of the vertebrate fauna
146 (Parker and Martz, 2009, 2011), and perhaps a significant change in flora and paleoclimate
147 (Reichgelt et al., 2013; Nordt et al., 2015; Baranyi et al., 2017). U-Pb (CA-TIMS/zircon) ages from
148 the Sonsela Member range from ~220 to ~214 Ma (Ramezani et al., 2011; [Marsh et al., 2019](#);
149 [Rasmussen et al., 202019](#)) from below the siliceous horizon and from ~214 to ~213 Ma
150 (Ramezani et al., 2011; Nordt et al., 2015; Kent et al., 2018; [Rasmussen et al., 202019](#)) from
151 above.

152 Overlying the conglomeratic sandstones of the Sonsela Member is a purplish mudstone that
153 marks the base of the Petrified Forest Member (Fig. 2). This member consists of red and purple
154 mudstone with abundant paleosols and pedogenic carbonate nodules, with local conglomeratic
155 sandstone beds that formed in bedload-dominated streams. Near the top of the unit is the
156 Black Forest bed, which consists of limestone-pebble conglomerate and reworked andesitic tuff
157 (Ash, 1992). Zircon grains from the Black Forest bed have yielded U-Pb (ID-TIMS or CA-TIMS)
158 ages of ~213 Ma to ~210 Ma (Riggs et al., 2003; Heckert et al., 2009; Ramezani et al., 2011; Kent
159 et al., 2018; [Rasmussen et al., 202019](#)).

160 **3. SAMPLED HORIZONS**

161 We analyzed detrital zircon grains from twenty-nine samples collected from the Permian and
162 Triassic strata described above. Samples include one from the Coconino Sandstone, five from
163 the Moenkopi Formation (one that may be from the Wupatki Member and four from the
164 Holbrook Member), and twenty-three from the Chinle Formation (one from the Mesa Redondo
165 Member, three from the Blue Mesa Member, twelve from the Sonsela Member, and seven
166 from the Petrified Forest Member). Approximate stratigraphic positions of the samples are
167 shown on Figure 2, lithic characteristics are described in DR Table 1, and images of the sampled
168 material (both core and thin sections) are presented in Appendix 1. Each sample consisted of 20
169 cm (for sandstone) to 30 cm (for mudstone-siltstone) of $\frac{1}{4}$ sections of the core.

170 **4. ANALYTICAL AND INTERPRETIVE METHODS**

171 Zircon mineral separation was performed at the Arizona LaserChron Center
172 (www.laserchron.org) using methods modified from those outlined by Gehrels (2000), Gehrels
173 et al. (2008), and Gehrels and Pecha (2014) because of the small size of all samples and the
174 abundance of clay minerals in many samples. The process included using a hand-crusher to
175 break the samples apart, a gold pan for initial density separation, and an ultrasonic disruptor

176 (Hoke et al., 2014) to separate zircon crystals from clay mineral grains. Magnetic separation was
177 performed with a Frantz Isodynamic separator, followed by density separation using methylene
178 iodide.

179 Zircon grains greater than 60 μm in size were enclosed in 1-inch epoxy mounts along with
180 fragments of zircon standards SL (primary) and FC-1 and R33 (secondary). Mounts were
181 polished approximately 5-10 μm deep to expose the internal structure of the grains but retain
182 as much material as possible for subsequent CA-TIMS analysis. Imaging was performed with a
183 backscatter electron detector system (BSE) using a Hitachi S3400 scanning electron microscope
184 (SEM) to ensure analysis of zircon and to avoid inclusions and fractures. Mounts were cleaned
185 with 1% HCl and 1% HNO_3 prior to isotopic analysis.

186 U-Pb isotopic analyses were conducted by LA-ICPMS using a Teledyne/Photon Machines
187 Analyte G2 laser connected to a Thermo Element2 mass spectrometer. Analyses utilized a 20
188 μm diameter laser beam fired at 7 hz for 15 seconds, resulting in 10-12 μm deep pits. Details of
189 the analytical methods are reported in DR Table 2.

190 U-Pb ages are calculated with an in-house data-reduction routine (E2agecalc) following
191 methods of Pullen et al. (2018). Analyses of zircon grains from our samples are reported in DR
192 Table 3, with results filtered for discordance (using cutoffs of 80% and 105% concordance),
193 precision (10%), and common Pb (>600 cps counts of 204). Following the recommendations of
194 Horstwood et al. (2016), uncertainties for individual analyses include only internal (random or
195 measurement) uncertainty contributions, whereas uncertainties of pooled ages contain both
196 internal and external (systematic) contributions.

197 Detrital age distributions are displayed and analyzed with normalized probability density plots,
198 which are based on the individual ages and measured uncertainties from each sample.
199 Provenance interpretations are based on the main clusters of ages, with less emphasis on ages
200 that do not belong to clusters given the possibility that they are unreliable due to Pb loss,
201 inheritance, analysis of inclusions, high common Pb, or unusual Pb/U fractionation due to
202 ablation along fractures (Gehrels, 2014).

203 Analysis of provenance is conducted by comparison with age distributions from five likely
204 source regions for Permian-Triassic strata of the Colorado Plateau, which include the
205 Appalachian orogen, the Ouachita orogen, local basement rocks of southwestern Laurentia, the
206 East Mexico arc, and the Permian-Triassic magmatic arc developed along the Cordilleran margin
207 of southwestern North America (Fig. 1; Dickinson, 2018). The age distributions for these regions
208 include data from: (1) upper Paleozoic strata of the Appalachian foreland basin (Thomas et al.,
209 2017) and Illinois and Forest City basins (Kissock et al., 2018), (2) upper Paleozoic strata of the
210 Delaware (Xie et al., 2018), Fort Worth (Absalem et al., 2018), and Marathon (Thomas et al.,
211 2019) basins, (3) lower Paleozoic strata of the Grand Canyon (Gehrels et al., 2011) and
212 Cordilleran passive margin strata in southern California and northern Sonora (Gehrels and
213 Pecha, 2014), (4) Permian and Triassic strata of the Barranca and El Antimonio Formations of

214 Sonora (Gonzalez-Leon et al., 2009; Gehrels and Pecha, 2014), Jura-Cretaceous strata of the
215 Great Valley (DeGraaff-Surpless et al., 2002; Surpless et al., 2006; Wright and Wyld, 2007),
216 Permian-Triassic igneous rocks in California (Chen and Moore, 1982; Miller et al., 1995; Tobisch
217 et al., 2000; Barth and Wooden, 2006, 2011, 2013; Saleeby and Dunne, 2015), and (5) Mesozoic
218 strata that accumulated adjacent to the East Mexico arc (Ortega-Flores et al., 2014). Age
219 distributions for these five regions are presented in Figure 3.

220 Comparisons of age distributions are quantified using several different statistical measures that
221 examine the degree to which age distributions contain similar proportions of similar age
222 groups. Five metrics used in this study include the cross-correlation coefficient, values of
223 similarity and likeness, and the Kolmogorov-Smirnov (K-S) D values and Kuiper V values. The
224 statistical basis as well as strengths and limitations of each of these metrics are summarized by
225 Saylor and Sundell (2016), ~~and~~ [Wissink et al. \(2018\)](#), ~~and~~ [Vermeesch \(2018a\)](#). Results from
226 these comparisons are presented in DR Table 4. The interpretations offered below are based on
227 cross-correlation coefficients, although all five metrics yield similar results. Comparisons are
228 also presented visually through the use of multidimensional scaling (MDS) diagrams
229 (Vermeesch, 2013; Wissink et al., 2018), which provide a 2-dimensional representation of the
230 differences between multiple age distributions. MDS analyses are also based on cross-
231 correlation coefficients.

232 Maximum depositional ages are ~~determined from~~ ~~calculated~~ from estimates of the age of the
233 youngest distinct cluster of three or more overlapping ages (Dickinson and Gehrels, 2009;
234 Gehrels, 2014). The age of this cluster is estimated using four different methods, each of which
235 have strengths and limitations. Complications with these methods arise from (1) the need to
236 make unconstrained decisions about which analyses to include or exclude from consideration,
237 (2) the evidence from complicated PDP age distributions and high (>1.0) MSWD values that the
238 youngest clusters for most samples contain multiple age populations, (3) the evidence that
239 dates in some clusters have been compromised by Pb loss, and (4) issues of statistical
240 robustness for some methods (Vermeesch, 2018b). Following are short descriptions of the four
241 methods:

242 ~~, as described below.~~

- 243 • Age of the youngest peak on a probability density plot (PDP). This method is advantageous
244 because no decisions are made about which analyses are included/excluded, but it has the
245 disadvantage that no uncertainty is reported for the peak age.
- 246 • Weighted Mean age and uncertainty of the youngest cluster. This method calculates the
247 average age of a cluster by weighting each analysis according to the inverse-square of its
248 uncertainty. The reported uncertainty relates to the mean age (e.g., standard error of the
249 mean), not the age distribution of constituent analyses (e.g., standard deviation). An
250 advantage of this method is that it also yields a Mean Square of the Weighted Deviates
251 (MSWD), which is an indication of the degree to which the ages belong to a single
252 population (values of ~1 or less indicate a single population). A disadvantage of this method

253 is that the investigator must decide which ages are included in the calculation, which leads
254 to the possibility of subjective bias. In this study, clusters include the main set of continuous
255 ages, with boundaries selected at the youngest and oldest gap in ages. This calculation is
256 available from the Weighted Mean function in Isoplot (Ludwig, 2008).

- 257 • Tuffzirc age and uncertainty of the youngest cluster. This method uses the age extractor
258 function in Isoplot (Ludwig, 2008), which identifies the largest cluster of ages that overlap to
259 an acceptable degree (probability-of-fit > 0.05), reports the median value as the most likely
260 age, and uses the range of included ages to calculate an asymmetric uncertainty. The
261 reported uncertainty refers to the median value (not the range of constituent analyses).
262 Excluded ages are interpreted to pre-date the selected cluster (if older), or to be
263 compromised by Pb loss (if younger). This method is advantageous in that no subjective
264 decisions are made about including/excluding ages.
- 265 • Maximum Likelihood age and uncertainty. This method uses a maximum likelihood analysis
266 to determine the gaussian distribution that best fits the youngest cluster. The reported
267 uncertainty refers to the most likely value (not the range of constituent analyses). This
268 method is advantageous in that no subjective decisions are made about including/excluding
269 ages. It is available from the Unmix function of Isoplot (Ludwig, 2008).

270

271 The results of these calculations are presented in DR Tables 3 and 6.

272 DR Table 6 also reports the age and uncertainty of the youngest analysis from each sample. This
273 youngest age does not provide a reliable maximum depositional age given that the youngest
274 age of a distribution will always be younger than the true age due to analytical uncertainty
275 (Gehrels, 2014). For example, [as described by Coutts et al. \(2019\)](#), consider the analytical data
276 from a population of zircon grains that have exactly the same true age. Because of analytical
277 uncertainty, the measured ages of half of the analyses will be younger than the true age, and
278 half will be older, and the youngest age will be significantly younger than the mean (true) age.
279 Ironically, the more grains analyzed, the greater the inaccuracy of this youngest age!

280 In addition to this statistical bias, the youngest single age will be even farther from the mean
281 (true) age if it has been compromised by Pb loss ([e.g., Andersen et al., 2019](#)). We report these
282 youngest ages because they provide important information about the possibility that analyses
283 included in the youngest cluster have also experienced Pb loss. DR Table 6 accordingly reports
284 this youngest age (and uncertainty), as well as information about its U concentration, the
285 average U concentration of the youngest cluster of ages, and whether the youngest age belongs
286 to the youngest cluster or is an outlier. U concentration is important because Pb loss is
287 commonly correlated with the degree of radiation damage, which is a function of U
288 concentration (and age).

289 A second test of the likelihood that analyses belonging to the youngest cluster have
290 experienced Pb loss is provided by a plot of U concentration versus age for analyses belonging
291 to the youngest cluster. Such plots are shown for every sample in DR Table 3, and whether a
292 correlation exists is indicated in DR Table 6.

293 Also included in DR Table 6 are the preferred age and uncertainty for each sample. The
294 preferred age is based on the average of the four age estimates ~~s~~ determined by peak age,
295 weighted mean, Tuffzirc, and Unmix analyses. The uncertainty of this preferred age is based on
296 the average of the uncertainty from each method, and is shown with both internal-only
297 uncertainties and with combined internal and external uncertainties.

298 The average precision of individual analyses reported herein is 2.3% (2σ) for $^{206}\text{Pb}^*/^{238}\text{U}$ dates
299 and 2.6% for $^{206}\text{Pb}^*/^{207}\text{Pb}^*$ dates. For pooled ages, calculated as described above, the average
300 precision is 0.52% (2σ) including only internal uncertainties and 0.98% (2σ) including both
301 internal and external sources of uncertainty. The accuracy of our analyses can be estimated
302 from the age of the secondary standards that were analyzed with each set of unknowns. As
303 reported in DR Table 7 and shown on Figure 4, sets of $^{206}\text{Pb}^*/^{238}\text{U}$ dates for FC-1 are offset
304 between +0.25% and -0.45% from the reported $^{206}\text{Pb}^*/^{238}\text{U}$ date of 1099.9 Ma (Paces and
305 Miller, 1993), with an average offset for all 1,065 analyses of +0.03%. For R33, offsets range
306 from +0.85% to -0.95% from the assumed age of 419.3 Ma (Black et al., 2004), with an average
307 offset for all 291 ages of -0.23%. MSWD values for the sets of FC-1 and R33 ages are 0.95 and
308 0.92 (respectively) – this demonstrates that reported uncertainties for individual analyses are
309 accurate, and that MSWD values for sets of unknown ages are reliable indicators of the
310 existence of multiple age components.

311 Interpretation of our ages relative to the Geologic Time Scale is based on the August 2018
312 version of the International Chronostratigraphic Chart (Cohen et al., 2013).

313 U-Pb geochronology by LA-ICPMS also provides U concentrations and U/Th values for each
314 analysis, which can be used as a geochemical fingerprint of detrital zircon grains (e.g., Gehrels
315 et al., 2006, 2008; Riggs et al., 2012, 2016). This information is accordingly reported for each
316 analysis in DR Table 3, and for each set of analyses in DR Table 6.

317 **5. U-Pb GEOCHRONOLOGIC RESULTS**

318 Results of our U-Pb geochronologic analyses are described below, keyed to the age
319 distributions for individual samples that are shown on Figures 5, 6, and 7. Figure 8 presents age
320 distributions for combined sets of samples. Age distributions from all of the samples are
321 compared statistically in DR Table 4 using the five metrics described above, and MDS plots are
322 shown in Figure 9.

323 We note that Rasmussen et al. (202019) have reported a subset of the LA-ICPMS ages
324 presented herein. The ages reported in their study are for the grains selected for CA-TIMS
325 analysis, which in most cases are among the youngest grains in each of our samples (as
326 documented in Appendix 2). This strategy was followed assuming that these grains represent
327 the youngest age components in each sample, and accordingly provide the most useful
328 maximum depositional ages. The individual dates reported in the two studies are identical, but,
329 given the selection process noted above, the pooled ages reported by Rasmussen et al.

330 (202019) are consistently younger than the pooled ages reported herein. A comparison of the
331 results of the two studies is summarized in Appendix 2. The discussions below are based on the
332 full set of ages from each sample.

333 Sample numbers are registered to the CPCP core (CPCP-PFNP13-1A) by the number of the core
334 run and segment (e.g., our sample number 383-2 is from CPCP-PFNP13-1A-383Y-2, which
335 specifies that the material is from run 383, segment 2). The part of each segment that was
336 collected for geochronologic analysis is specified in DR Table 1.

337 **5.1 Coconino Sandstone**

338 Our sample from quartz arenite of the lower Permian (Leonardian) Coconino Sandstone
339 (sample 390-1) yielded 285 acceptable ages (DR Table 3; Figure 4). Most grains belong to two
340 broad age groups of ~2.0-1.0 Ga and ~640-295 Ma. Individual age peaks are at 2712, 1898,
341 1746, 1646, 1497, 1432, 1347, 1162, 1038, 667, 612, 590, 552, 476, 430, 419, 391, 374, 355,
342 341, and 300 Ma.

343 **5.2 Moenkopi Formation**

344 Five samples from the Lower-Middle Triassic Moenkopi Formation have been analyzed (Fig. 2).
345 The lowest sample (383-2) is assigned to the Wupatki Member based on the red-brown
346 laminated mudstone to fine-grained sandstone lithology (Fig. 2; Table DR 1). The age
347 distribution from this sample is very similar to that found in underlying upper Paleozoic strata,
348 with two dominant age groups from ~2.2 Ga to 1.0 Ga and from ~680 Ma to 250 Ma (Fig. 5).
349 Although the preferred interpretation for this sample is that it belongs to the lowest part of the
350 Moenkopi Formation, an alternative is that the sample is late Paleozoic in age, and perhaps
351 correlative with fine-grained clastic strata (e.g., the Toroweap Formation) that regionally overlie
352 the Coconino Sandstone. In an effort to provide a comparison with underlying and overlying
353 strata, the results from this sample are shown on Figures 5 and 6. Additional studies of the
354 sampled horizon are needed to resolve whether this sample belongs to the Moenkopi
355 Formation or underlying upper Paleozoic strata.

356 The upper four samples (349-3, 335-1, 327-2, and 319-2) are all from sandstone, siltstone, and
357 mudstone of the Holbrook Member. These samples yield generally similar age distributions
358 (average CCC of 0.24; DR Table 4), with significant proportions of ~1.42 Ga, 650-510 Ma, 290-
359 270 Ma, and 250-235 Ma ages (Fig. 6). With ages from all four Moenkopi Formation samples
360 combined, PDP peak ages are 1420, 594, 543, 285, and 250 Ma (Fig. 8). As shown in Figures 9B
361 and 9C, age distributions from the lower two samples (349-3 and 335-1) and upper two samples
362 (327-2 and 319-2) form two distinct groups. These clusters are also apparent from CCC values of
363 0.83 and 0.24 for the lower and upper samples (respectively), in comparison with a low average
364 value (0.08) for comparison of the two sets with each other (DR Table 4).

365 **5.3 Chinle Formation**

366 Twenty-three samples from the Mesa Redondo Member, Blue Mesa Member, Sonsela Member,
367 and Petrified Forest Member of the Chinle Formation have been analyzed (Fig. 2). Results from
368 each member are described separately below.

369 **5.4 Mesa Redondo Member**

370 One sample of sandstone from the Mesa Redondo Member (305-2) yields dominant age groups
371 of ~2.0-1.6 Ga, 1.44 Ga, 1.1-1.0 Ga, 750-500 Ma, and 450-300 Ma, and 290-220 Ma (Fig. 7), with
372 PDP peak ages of 1443, 1036, 618, 412, 323, 248, and 223 Ma. As reported in DR Table 4 and
373 shown on Figure 9C, the >240 Ma ages in this samples resemble ages in the underlying
374 Moenkopi Formation and Coconino Sandstone.

375 **5.5 Blue Mesa Member**

376 Three samples (297-2, 287-2, 261-1) of siltstone and mudstone from the Blue Mesa Member
377 yield very similar results, with nearly identical <240 Ma ages and small but varying proportions
378 of ~1.64 Ga, 1.44 Ga, 1.1-1.0 Ga, 650-500 Ma, and 440-240 Ma ages (Figures 7 and 8). Both
379 <240 Ma ages (Fig. 9A) and >240 Ma ages (Fig. 9C) differ from those in underlying strata of the
380 Mesa Redondo Member. Between 56% and 89% of the grains analyzed from these samples
381 yield ages between 232 and 210 Ma, with PDP peak ages of 221-220 Ma (Fig. 7; DR Table 6).
382 With all three samples combined, 62% of the ages are <240 Ma, and PDP peak ages are 1630,
383 1440, and 220 Ma (Fig. 8).

384 **5.6 Sonsela Member**

385 Twelve samples (243-3 to 158-2) from the Sonsela Member yield two different sets of age
386 distributions (Figures 7, 8, and 9; DR Table 3). The lower six samples (243-3 to 196-3), all
387 consisting of sandstone and subordinate siltstone (DR Table 1), yield small numbers of
388 Precambrian grains that are mostly ~1.65 and 1.44 Ga, with few ~1.1-1.0 Ga grains. These
389 samples yield between 53% and 79% ages <240 Ma, with most ages between 234 and 208 Ma,
390 and PDP peak ages of 221-218 Ma (Fig. 7). With ages from all six samples combined, 68% of the
391 grains are <240 Ma, and PDP peak ages are 1650, 1445, 1084, and 219 Ma (Fig. 8). Comparison
392 of age distributions (Figures 7 and 8), CCC values (DR Table 4), and MDS patterns (Fig. 9)
393 suggests that the <240 Ma ages in these strata are indistinguishable from <240 Ma ages in
394 underlying Blue Mesa strata, whereas >240 Ma ages in the two sets of samples are less similar
395 due to the variability of ages from the three Blue Mesa Member samples. Ages that are >240
396 Ma in these strata have even less similarity to ages from the Mesa Redondo Member,
397 Moenkopi Formation, and Coconino Sandstone (Fig. 9; DR Table 4).

398 The upper six samples from the Sonsela Member (195-2 to 158-2) consist mainly of sandstone
399 and subordinate siltstone (DR Table 1). All six samples yield a subordinate but consistent
400 proportion of Precambrian ages that are mostly ~1.43 and 1.1-1.0 Ga, with few 1.65 Ga grains
401 (Fig. 7). Grains with ages of <240 Ma comprise between 39% and 77% of the grains analyzed.
402 These ages are somewhat younger than in lower Sonsela Member samples, with PDP peak ages

403 of 217-214 Ma. With all six samples combined, 50% of the grains are <240 Ma, and PDP peak
404 ages are 1643, 1434, 1082, 256, and 215 Ma (Fig. 8).

405 Statistical analysis (MDS patterns in Figure 9 and CCC values in DR Table 4) shows that the <240
406 Ma ages in upper and lower Sonsela Member strata are significantly different, whereas >240
407 Ma ages are less distinct. Exceptions to this are >240 Ma ages in sample 243-3 (lower Sonsela
408 Member), which resemble equivalent ages in strata of the upper Sonsela Member (Fig. 9C), and
409 <240 Ma ages in sample 196-3, which share characteristics with strata of both the upper and
410 lower Sonsela Member (Fig. 9A). Ages from strata of the upper Sonsela Member show even less
411 overlap with ages from strata of the Blue Mesa Member and underlying units (Fig. 9 and DR
412 Table 4).

413 **5.7 Petrified Forest Member**

414 Seven samples (131-2 to 52-2) from the Petrified Forest Member were collected mainly from
415 claystone, mudstone, siltstone, and fine-grained sandstone, with only the lowest sample (131-
416 2) consisting of coarse-grained sandstone. The upper six fine-grained samples yield between
417 17% and 72% <240 Ma ages that are significantly younger than in underlying strata, with PDP
418 peak ages between 212 and 209 Ma. Ages that are >240 Ma in these samples differ from
419 equivalent ages in strata of the Blue Mesa Member and Sonsela Member, but overlap to
420 varying degrees with ages in strata of the Mesa Redondo Member, Moenkopi Formation, and
421 Coconino Sandstone (Fig. 9C; DR Table 4). With the six samples combined, 35% of the grains are
422 <240 Ma, and PDP peak ages are 1636, 1430, 1032, 629, 379, 287, and 209 Ma (Fig. 8). The
423 lowest sample (131-2), consisting of coarse-grained sandstone, differs from the other Petrified
424 Forest Member samples, with an age peak of 221 Ma, and a greater proportion (68%) of >240
425 Ma ages (Fig. 7). The <240 Ma ages are very similar to equivalent ages in strata of the lower
426 Sonsela Member (Fig. 9A; CCC=0.97), whereas >240 Ma ages are more similar to ages in the
427 upper Sonsela Member (CCC=0.72) than in the lower Sonsela Member (CCC=0.59) (Fig. 9C).

428 **5.8 Summary of Chinle results**

429 The patterns of LA-ICPMS ages described above suggest that the studied part of the Chinle
430 Formation comprises four different units, each of which has a distinct chronologic signature for
431 both <240 Ma and >240 Ma ages (Fig. 8). These chronostratigraphic units correspond to the
432 Mesa Redondo Member, Blue Mesa Member and lower part of the Sonsela Member, upper
433 part of the Sonsela Member, and Petrified Forest Member.

434 **6. U AND Th GEOCHEMISTRY OF CHINLE ZIRCON GRAINS**

435 In an effort to evaluate whether the Triassic zircon grains from the four chronostratigraphic
436 units also have distinct chemical signatures [following Riggs et al. (2012, 2016)], Figure 10
437 summarizes the U concentrations and U/Th values for Triassic zircon grains analyzed from each
438 unit. The patterns exhibited in these plots suggest that (1) zircon grains from the Mesa
439 Redondo Member are significantly different from zircon grains in overlying strata, (2) grains in

440 strata of the Blue Mesa Member and lower Sonsela Member differ from grains in overlying
441 strata of the upper Sonsela Member and Petrified Forest Member, and (3) grains in strata of the
442 upper Sonsela Member and Petrified Forest Member have distinctive and slightly different
443 bimodal patterns. Plots showing U concentrations and U/Th values for individual samples are
444 included in DR Table 3.

445 **7. PROVENANCE INTERPRETATIONS**

446 Detrital zircon geochronology has previously been used to reconstruct the provenance of
447 Permian and Triassic strata of the Colorado Plateau by Riggs et al. (1996, 2003, 2012, 2013,
448 2016), Dickinson and Gehrels (2003, 2008), Gehrels et al. (2011), Lawton et al. (2015), and
449 Marsh et al. (2019). The results of most of these geochronologic studies, and a large number of
450 stratigraphically based analyses, have recently been summarized by Dickinson (2018). The
451 following sections compare our new results with this existing information.

452 The following comparisons are based in part on qualitative comparison of age distributions of
453 the strata that we have analyzed and of age distributions from five potential source areas
454 (summarized on Figure 3). As described by Gehrels (2000), such comparisons focus on the
455 degree to which two age distributions contain similar proportions of similar ages. Comparisons
456 are also based on the results of statistical analyses (DR Table 4) that compare our results with
457 the age distributions of possible source areas, and on graphic displays of these comparisons
458 using MDS plots (Fig. 9).

459 **7.1 Coconino Sandstone**

460 Lawton et al. (2015) and Dickinson (2018) suggest that lower Permian strata of the Colorado
461 Plateau comprise a regional blanket of eolian strata that was shed predominantly from the
462 Appalachian and/or Ouachita orogens, with increasing input in northern regions from local
463 basement rocks exposed in the Uncompahgre or Ute Uplift (Fig. 1). These interpretations are
464 supported by the age distributions shown on Figures 5 and 11, with southern strata (Coconino,
465 Cedar Mesa, and White Rim sandstones) forming a distinct group dominated by
466 Appalachian/Ouachita detritus, and northern strata (Castle Valley and Cutler strata) forming a
467 separate group with increasing proportions of ca 1.44 Ga grains. The age distribution from our
468 Coconino Sandstone sample (390-1) fits well with other strata from the southern Colorado
469 Plateau in having abundant 1.2-1.0 and 670-300 Ma grains and a low proportion of ~1.44 Ga
470 grains (Figures 5 and 11; DR Table 4).

471 **7.2 Moenkopi Formation**

472 As summarized on Figure 6, the detrital zircon ages from our four Holbrook Member samples
473 are generally similar to ages from a Holbrook Member sandstone reported by Dickinson and
474 Gehrels (2008). Dominant >300 Ma age groups and interpreted source terranes include ~1.44
475 Ga and subordinate ~2.0-1.6 Ga grains derived from Laurentian Precambrian basement and
476 ~670-300 Ma grains derived from Ouachita/Gondwana sources. Based on comparison with

477 detrital zircon ages from strata that accumulated in proximity to the East Mexico and southern
478 Cordilleran arcs (Fig. 3), 300-260 Ma grains (PDP peak ages of 285, 284, 265, 260, and 279) are
479 interpreted to have been shed from the East Mexico arc (peak age of 284 Ma), whereas 260-
480 230 Ma grains (peak ages of 250, 248, 228, 245, and 239 Ma) were likely shed from Early-
481 Middle Triassic parts of the Cordilleran magmatic arc in California and northwestern Mexico
482 (peak ages of 243, 236, and 226 Ma) (Fig. 3). Statistical analyses (DR Table 4) suggest nearly
483 equal contributions from the Ouachita orogen, local basement rocks, and the East Mexico arc.

484 More detailed analysis of the age distributions (Fig. 6) and MDS patterns (Fig. 9) suggest that
485 the lower two samples (349-3 and 335-1) [plus sample CP8 of Dickinson and Gehrels (2008)] are
486 dominated by ~1.44 Ga and ~285 Ma grains, whereas the upper two samples (327-2 and 319-2)
487 are dominated by ~620-590 Ma and ~250-230 Ma grains. The age distributions (Fig. 6) and
488 comparison metrics (Fig. 9; DR Table 4) suggest that the lower samples were shed mainly from
489 local basement rocks (CCC=0.30) and the East Mexico arc (CCC=0.22), whereas the upper
490 samples were shed largely from the Ouachita orogen (CCC=0.23).

491 **7.3 Chinle Formation**

492 Our results from detrital zircon grains recovered from strata of the Chinle Formation are
493 consistent with the provenance and paleogeographic reconstructions offered by Riggs et al.
494 (1996, 2003, 2012, 2013, 2016), Dickinson (2018), and Marsh et al. (2019). Given the observed
495 age distributions (Fig. 7) and the location of our study site relative to Late Triassic
496 paleogeographic and paleotectonic features of southwestern North America (Fig. 12), likely
497 sources for pre-Triassic grains include rocks exposed in the Ouachita orogen to the southeast
498 and the Ancestral Mogollon highlands to the south and southwest. Given the abundance of ash
499 layers, bentonitic mudstone, and near-depositional-age zircon grains in strata of the Chinle
500 Formation, and the existence of arc-related plutons and volcanic rocks of Triassic age in Sonora
501 and southern California (Barth and Wooden, 2006, 2011, 2013; Saleeby and Dunne, 2015; Riggs
502 et al., 2016), Stewart et al. (1986), Riggs et al. (2012, 2016), Dickinson (2018), Marsh et al.
503 (2016), and many other researchers conclude that Triassic grains in Chinle strata were derived
504 from the active arc built along the southern Cordilleran margin. The occurrence in fore-arc and
505 back-arc strata of very similar distributions of ages (Fig. 3) is inconsistent with interpretations
506 (e.g., Hildebrand, 2009, 2013) that the early Mesozoic arc was located far from southwestern
507 North America.

508 Although our data are entirely consistent with the provenance interpretations outlined above,
509 the density of our sampling and the large number of analyses from most samples provide
510 opportunities to reconstruct temporal changes in Triassic provenance in greater detail, and with
511 the benefit of statistical analyses to quantify conclusions. Following are interpretations based
512 on strata belonging to each of the different members of the Chinle Formation.

513 **7.4 Mesa Redondo Member**

514 The provenance of strata belonging to the Mesa Redondo Member is similar to that of the
515 underlying Moenkopi Formation, with our sample (305-2) containing abundant ~640-300 Ma
516 grains derived from Ouachita/Gondwana sources as well as ~290-260 Ma grains derived from
517 the East Mexico arc (Fig. 8). Statistical analysis confirms higher similarity of >240 Ma grains with
518 Ouachita sources (0.58) than with Appalachian (0.35) or local basement (0.15) sources (DR
519 Table 4). This sample also yields a significant proportion of Triassic ages that approximate the
520 depositional age for these strata (Fig. 7). These young grains, with a PDP age peak of 223 Ma,
521 are interpreted to have been transported primarily by aeolian processes from the active
522 magmatic arc to the west (Fig. 12). Statistical analysis demonstrates that the Triassic ages in
523 these samples are significantly different from ages in overlying strata (Fig. 9A) and that the
524 >240 Ma ages are similar to those in strata of the Petrified Forest Member (Fig. 9C).

525 **7.5 Blue Mesa Member**

526 Our three samples from strata of the Blue Mesa Member yield a large proportion of Triassic
527 zircon grains (Figures 7 and 8) that were derived from the active Cordilleran magmatic arc to
528 the west (Fig. 12), and a small proportion of pre-240 Ma grains that were shed from local
529 basement rocks and the Ouachita and/or Appalachian orogens (Fig. 8). Statistical analysis
530 confirms that the Triassic ages in all these samples are quite similar (Fig. 9A), whereas the age
531 distributions of >240 Ma grains in the three samples are more variable (Fig. 9C; DR Table 4).

532 **7.6 Lower Sonsela member**

533 The lower six samples from the Sonsela Member yield a large proportion of Triassic grains
534 derived from the Cordilleran magmatic arc, and fewer ages derived from local basement rocks
535 and Ouachita/Gondwana sources (Figures 7 and 8). Distinctive among the older grains is a
536 significant proportion of ~1.44 Ga grains that ~~most likely may have been incorporated during~~
537 ~~transport from the Ouachita orogenic highlands, or may~~ signal increased input from the
538 Ancestral Mogollon highlands to the southwest (Marsh et al., 2019) (Fig. 12). MDS analysis
539 demonstrates that the <240 Ma and >240 Ma ages in these samples are quite similar, with the
540 only significant difference being the larger number of ~1.1 Ga grains in sample 243-3 (Figures 7
541 and 9C).

542 **7.7 Upper Sonsela Member**

543 The upper six samples from the Sonsela Member reveal a continued low contribution from the
544 Ouachita orogen, and a significant increase in the proportion of ~1.08 Ga and 260-240 Ma
545 grains (Figures 7 and 8). The ~260-240 Ma grains were likely derived from Permian-Early Triassic
546 igneous rocks along the southern Cordilleran margin (Saleeby and Dunne, 2015; Riggs et al.,
547 2016), exposed in the Ancestral Mogollon Highlands (Fig. 12). The prominent ~1.44 and 1.08 Ga
548 grains in these samples may also have been shed from highland sources to the south and
549 southwest. Triassic grains in these samples record a slightly younger (230 to 204 Ma, peak age
550 of 215 Ma) phase of magmatism along the Cordilleran margin. Significant changes in both <240
551 Ma and >240 Ma ages occur between samples 196-3 and 195-2 (Figure 7). MDS analysis

552 demonstrates that patterns of both <240 Ma and >240 Ma ages are consistent among the six
553 upper Sonsela Member samples, but are distinct from ages in all other parts of the Chinle
554 Formation (Figures 7 and 9).

555 **7.8 Petrified Forest Member**

556 Strata of the Petrified Forest Member record an important shift in provenance, with
557 significantly greater detrital input from the East Mexico arc (~287 Ma) and the Ouachita orogen
558 (~640-300 Ma), and a broader range of >1.0 Ga basement sources (Figures 7 and 8). Triassic
559 grains in these strata are also significantly younger, with ages of 228 to 200 Ma (peak age of
560 209 Ma).

561 An exception to these patterns is recorded by ages from the coarse-grained sandstone of
562 sample 131-2, which has Precambrian grains that are mainly ~1.1-1.0 and 1.44 Ga (like upper
563 Sonsela Member; Fig. 9B), and Triassic grains that are ~221 Ma (like strata of the lower Sonsela
564 Member and Blue Mesa Member; Fig. 9A). This lower Petrified Forest Member sample is
565 interpreted to have been reworked mainly from lateral equivalents of underlying strata of the
566 Sonsela Member and Blue Mesa Member, with little or no input from the active arc to the west.
567 MDS analysis shows that sample 116-1 contains a mix of these older reworked grains and the
568 younger grains present in overlying strata (Fig. 9A).

569 **8. MAXIMUM DEPOSITIONAL AGES**

570 The depositional age of Triassic strata on the Colorado Plateau is of considerable interest
571 because of the rich faunal and paleoclimatic records preserved within the Moenkopi Formation
572 and Chinle Formation, and as the zircon-based geochronological framework for the early
573 Mesozoic when coupled with paleomagnetic polarity stratigraphy and astrochronology (Olsen
574 et al., 2018, 2019; Kent et al., 2018, 2019; Rasmussen et al., 202019). There accordingly have
575 been many prior attempts to determine the depositional age of these strata by dating igneous
576 zircon grains in ash beds or volcanic cobbles and detrital zircon grains in clastic strata (e.g.,
577 Riggs et al., 1996, 2003, 2012, 2013, 2016; Heckert et al., 2009; Dickinson and Gehrels, 2009;
578 Irmis et al., 2011; Ramezani et al., 2011, 2014; Atchley et al., 2013; Nordt et al., 2015). As part
579 the Colorado Plateau Coring Project, Kent et al. (2018) and Rasmussen et al. (202019) report
580 the results of CA-TIMS analyses on many of the same samples reported herein. All of the
581 available CA-TIMS ages, and the preferred age models of Kent et al. (2019) and Rasmussen et al.
582 (202019), are shown on Figure 13.

583 Maximum depositional ages (MDA's) have been calculated from the LA-ICPMS ages using four
584 different methods (described above), with results presented in DR Tables 3 and 6 and shown
585 graphically on Figure 13. In the following discussion we assume that the average of the ages
586 and uncertainties calculated using these four different methods yields the most reliable
587 maximum depositional age available from our LA-ICPMS data. These preferred ages are
588 reported in DR Table 6, shown on Figure 13, and described below with 2σ uncertainties

589 incorporating only internal contributions (for inter-sample comparison) and incorporating both
590 internal and external uncertainty contributions (for comparison with ages from other studies)
591 (e.g., $224.4 \pm 2.0/2.7$ Ma).

592 The possibility that a maximum depositional age has been compromised by Pb loss is evaluated
593 by determining whether there is a correlation between U concentration and age. One criterion
594 is whether the youngest single age has higher U concentration than the average of the
595 youngest cluster – if yes than the youngest analysis (and perhaps other analyses within the
596 youngest cluster) may have experienced Pb loss. A second criterion is whether analyses within
597 the youngest cluster display an inverse correlation between U concentration and age – if yes,
598 then the higher U and younger analyses within the cluster may have experienced Pb loss.
599 Rasmussen et al. (202019) document Pb loss in zircon grains from several of our samples by
600 showing that CA-TIMS ages are commonly older than LA-ICPMS ages from the same crystals.

601 **8.1 Coconino Sandstone**

602 Our analyses do not provide a useful maximum depositional age for strata of the Coconino
603 Sandstone (sample 390-1) because few late Paleozoic ages were recovered from this sample.

604 **8.2 Holbrook Formation of the Moenkopi Formation**

605 Of our four samples from the Holbrook Member of the Moenkopi Formation, three yield
606 preferred MDA's that young upward from $249.5 (\pm 1.6/2.5)$ Ma to $248.4 (\pm 2.0/2.8)$ Ma to 245.7
607 $(\pm 1.9/2.7)$ Ma (DR Table 6). These MDA's are consistent with the inferred Early-Middle Triassic
608 age of the strata and the corresponding ~ 251 - 237 Ma range for Early and Middle Triassic time
609 on the Geologic Time Scale (Cohen et al., 2013). All three samples show patterns of U
610 concentration that suggest the possibility of Pb loss (DR Table 6).

611 **8.3 Mesa Redondo Member of the Chinle Formation**

612 Our one sample (305-2) from strata of the Mesa Redondo Member yields a preferred MDA of
613 $223.3 \pm 1.3/2.2$ Ma (DR Table 6). A low MSWD value (0.5) suggests that all ages belong to the
614 same age population, and patterns of U concentration do not indicate the presence of Pb loss.
615 This MDA overlaps with CA-TIMS ages of ~ 224.7 - 221.7 Ma from the same sample but is older
616 than the preferred single-grain age of ~ 221.7 Ma (Rasmussen et al., 202019). The LA-ICPMS
617 MDA of $223.3 \pm 1.3/2.2$ is significantly younger than CA-TIMS ages of ~ 225.2 Ma (Ramezani et
618 al., 2011) and ~ 227.6 (Atchley et al., 2013) from outcrop samples of the Mesa Redondo
619 Member.

620 **8.4 Blue Mesa Member of the Chinle Formation**

621 Our three samples (297-2, 287-2, 261-1) from strata of the Blue Mesa Member yield preferred
622 MDA's of $220.6 \pm 0.6/2.1$, $220.2 \pm 1.3/2.2$, and $220.7 \pm 1.3/1.9$ Ma (DR Table 6). All samples
623 yield MSWD values >1.0 (average of 2.4), which documents the presence of multiple age
624 populations. Patterns of U concentration suggest the presence of Pb loss in all three samples.

625 As shown on Figure 13, these ages are similar to most CA-TIMS ages from strata of the Blue
626 Mesa Member. From lower strata, our ages are slightly younger than a CA-TIMS age of ~ 221.8
627 Ma [from sample 297-2; Rasmussen et al. (202019)], indistinguishable from a CA-TIMS age of
628 ~ 220.5 Ma [from sample 287-2; Rasmussen et al. (202019)], ~~and similar to an ID-TIMS age of~~
629 ~~~ 220.9 Ma [from outcrop; Heckert et al. (2009)]~~. From upper strata, our age is similar to a CA-
630 TIMS age from outcrop of ~ 220.1 Ma (Atchley et al., 2013) but significantly younger than a CA-
631 TIMS age of ~ 223.0 Ma (Ramezani et al., 2011), also from outcrop.

632 **8.5 Lower part of the Sonsela Member**

633 Our six samples from the lower part of the Sonsela Member (243-3 to 196-3) yield preferred
634 MDA's of $220.3 \pm 0.9/1.8$ Ma (sample 243-3), $220.6 \pm 0.5/1.8$ Ma (sample 227-3), $220.5 \pm$
635 $0.6/1.6$ Ma (sample 215-2), $220.9 \pm 0.7/2.3$ Ma (sample 210-1), and $220.6 \pm 0.6/1.7$ Ma (sample
636 201-1). The sixth, uppermost sample (196-3) yields younger ages with a preferred MDA of 218.2
637 $\pm 0.7/1.6$ Ma. MSWD values for these samples are all high (average of 2.6), which demonstrates
638 the presence of multiple age components.

639 As shown on Figure 13, these MDA's are 1-3 m.y. older than most CA-TIMS ages from
640 equivalent strata. From oldest to youngest, the CA-TIMS ages include ~ 220.1 Ma [from outcrop;
641 Atchley et al. (2013)] from near the base, through ~ 218.8 Ma [sample 243-3; Rasmussen et al.
642 (202019)], ~ 217.7 Ma [sample 227-3; Rasmussen et al. (202019)], ~ 219.3 Ma [from outcrop;
643 Ramezani et al. (2011)], ~ 217.8 Ma [sample 215-2; Rasmussen et al. (202019)], ~ 218.0 Ma [from
644 outcrop; Ramezani et al. (2011)], and ~ 215.7 Ma and 214.4 Ma [samples 201-1 and 196-3;
645 Rasmussen et al. (202019)] at the top. The LA-ICPMS-based MDA's ages are also older than a
646 ~ 216.6 Ma MDA determined on LA-ICPMS ages from an outcrop sample of sandstone in the
647 middle part of the lower Sonsela Member, exposed ~ 132 km north of the CPCP core site (Marsh
648 et al., 2019).

649 **8.6 Upper part of the Sonsela Member**

650 The lower five samples from the upper Sonsela Member yield similar preferred MDA's of 215.4
651 $\pm 1.1/2.2$ Ma (sample 195-2), $216.5 \pm 0.7/1.9$ Ma (sample 188-2), $216.1 \pm 0.9/2.1$ Ma (sample
652 182-1), $215.1 \pm 0.8/1.9$ Ma (sample 177-1), and $216.6 \pm 1.0/2.0$ Ma (sample 169-1). An upper
653 sample yields a younger MDA of $213.8 \pm 0.6/2.1$ Ma (sample 158-2). All samples yield MSWD
654 values greater than 1.0 (average of 2.6), demonstrating the presence of multiple age
655 components. Most samples have patterns of U concentration that suggest the possibility of Pb
656 loss. The lower five MDA's are 2-3 m.y. older than CA-TIMS ages from equivalent strata, which
657 include outcrop ages of ~ 213.9 (Ramezani et al., 2011), ~ 213.6 Ma (Nordt et al., 2015), and
658 ~ 213.1 Ma (Ramezani et al., 2011), and CPCP core ages of ~ 214.0 Ma [samples 182-1 and 177-1;
659 Rasmussen et al. (202019)]. A CA-TIMS age of ~ 213.5 Ma for the upper sample [158-2;
660 Rasmussen et al. (202019)] is nearly identical to our age determination.

661 **8.7 Petrified Forest Member**

662 Our seven samples from the Petrified Forest Member yield three sets of preferred MDA's. The
663 lowest unit (sample 131-2) yields an MDA of $221.5 \pm 0.6/2.1$ Ma, which is significantly older
664 than MDA's in adjacent strata. Four samples near the middle of the unit yield similar preferred
665 MDA's of $211.5 \pm 3.1/3.4$ Ma (sample 116-1), $211.6 \pm 1.7/2.5$ Ma (sample 104-3), $211.2 \pm$
666 $1.2/1.9$ Ma (sample 92-2), and $211.7 \pm 1.0/2.0$ Ma (sample 84-2). These MDA's are very similar
667 to an ID-TIMS age of ~ 211.9 Ma (Irmis et al., 2011) from equivalent strata in outcrop. Two
668 upper samples, from the Black Forest bed, yield preferred MDA's of $209.6 \pm 3.0/3.4$ Ma (sample
669 66-1) and $209.8 \pm 0.5/1.6$ Ma (sample 52-2). These MDA's are similar to CA-TIMS ages of ~ 210.2
670 Ma from core [sample 52-2; Rasmussen et al. (202019)] and ~ 209.9 Ma from outcrop (Ramezani
671 et al., 2011), but are significantly younger than outcrop-based ID-TIMS ages of ~ 211.0 Ma
672 (Heckert et al., 2009) and ~ 213.0 Ma (Riggs et al., 2003). Most of our samples yield MSWD
673 values greater than 1.0 (average of 1.5), suggesting the presence of multiple age components,
674 and have patterns of U concentration that suggest the presence of Pb loss.

675 9. COMPARISON OF LA-ICPMS, CA-TIMS, AND MAGNETOSTRATIGRAPHIC CONSTRAINTS ON 676 DEPOSITIONAL AGE OF CHINLE FORMATION STRATA

677 ~~Our preferred maximum depositional ages for strata of the Chinle Formation range from ~ 223.3
678 to ~ 209.6 Ma, which is similar to the ~ 227.6 to ~ 209.9 Ma range of CA-TIMS ages (Fig. 13). All
679 available U-Pb data therefore suggest that the analyzed Chinle Formation strata are Late
680 Triassic, and probably Norian in age (Dickinson, 2018), given the assigned ages of ~ 237 to
681 ~ 201.3 for Late Triassic time (Cohen et al., 2013) and ~ 227 to ~ 208.5 Ma (Cohen et al., 2013) or
682 ~ 205.7 Ma (Kent et al., 2017) for Norian time.~~

683 ~~Figure 13 presents a comparison of our preferred maximum depositional ages, all available ID-
684 and CA-TIMS ages [from Riggs et al. (2003), Heckert et al. (2009), Ramezani et al. (2011), Irmis
685 et al. (2011), Atchley et al. (2013), Nordt et al., (2015), Kent et al. (2018), and Rasmussen et al.
686 (2019)], and two age models that are based on magnetostratigraphic and CA-TIMS
687 geochronologic information (Kent et al., 2019; Rasmussen et al., 2019). As shown on this figure,
688 our LA-ICPMS MDA's overlap with most CA-TIMS ages and both age models for most strata
689 belonging to the Blue Mesa Member and Petrified Forest Member, but are significantly older
690 for strata of the Sonsela Member. The following discussion explores this pattern of
691 convergence/divergence of the three chronometers—details of the magnetostratigraphic
692 information, CA-TIMS data, and age models are discussed by Kent et al. (2018, 2019) and
693 Rasmussen et al. (2019).~~

694 ~~Our preferred interpretation of the chronostratigraphic patterns is that U-Pb ages agree with
695 magnetostratigraphic ages for strata containing abundant zircon crystals which are air-fall in
696 origin, whereas U-Pb ages tend to predate deposition for strata that are dominated by zircon
697 grains recycled from older units. The difference in proportion of air-fall (near depositional age)
698 versus recycled (older) ages is interpreted to be controlled mainly by the grain size of the
699 sedimentary host, which is important because only >60 μm zircon grains were analyzed in this
700 study. Given that most detrital zircon grains transported with mud and silt are less than 60 μm~~

701 in diameter, zircon grains analyzed from mudstone-siltstone samples (and sequences) are
702 interpreted to be dominated by air-fall crystals rather than older recycled components. In
703 contrast, because coarser grained sediment is able to transport >60 μm zircon grains,
704 sandstone samples (and sequences) contain abundant recycled (older) zircon grains and a lower
705 proportion of air-fall (near depositional age) zircon grains.

706 Our LA-ICPMS ages from sandstones are significantly impacted by this difference because zircon
707 grains were selected for analysis at random in an effort to generate an unbiased age
708 distribution. CA-TIMS analyses from Chinle Formation sandstones have a higher yield of syn-
709 depositional ages because zircon grains were selected for analysis on the basis of their juvenile
710 appearance [e.g., acicular and prismatic crystals; Ramezani et al. (2011)] or from the youngest
711 grains in an LA-ICPMS data set (e.g., Rasmussen et al., 2019; Appendix 2).

712 These interpreted connections between stratigraphy, grain size, and proportions of air-fall
713 versus recycled zircon grains lead to the interpretation that the three chronometric records
714 agree (to within ~ 1 m.y.) for strata of the lower Blue Mesa Member and middle-upper Petrified
715 Forest Member because these units are dominated by mudstone and siltstone, resulting in U-
716 Pb ages mainly from air-fall (or slightly reworked) zircon grains. In contrast, LA-ICPMS ages from
717 the Sonsela Member significantly pre-date deposition because the dominant sandstones
718 contain abundant zircon grains recycled from slightly older units. For strata of the upper
719 Sonsela Member, CA-TIMS ages approximate the true depositional age because the methods of
720 grain selection were successful in identifying populations of air-fall zircon grains. For strata of
721 the lower Sonsela Member, however, these methods were unsuccessful in identifying a
722 sufficient number of air-fall zircon grains to determine a reliable depositional age, presumably
723 because of their low abundance relative to recycled grains.

724 Our preferred maximum depositional ages for strata of the Chinle Formation range from ~ 223.3 to
725 ~ 209.6 Ma, which is similar to the ~ 227.6 to ~ 209.9 Ma range of CA-TIMS ages (Fig. 13). All available U-
726 Pb data therefore suggest that the analyzed Chinle Formation strata are Late Triassic, and probably
727 Norian in age (Dickinson, 2018), given the assigned ages of ~ 237 to ~ 201.3 for Late Triassic time (Cohen
728 et al., 2013) and ~ 227 to ~ 208.5 Ma (Cohen et al., 2013) or ~ 205.7 Ma (Kent et al., 2017) for Norian time.

729 Figure 13 presents a comparison of our preferred maximum depositional ages, all available ID- and CA-
730 TIMS ages [from Riggs et al. (2003), Heckert et al. (2009), Ramezani et al. (2011), Irmis et al. (2011),
731 Atchley et al. (2013), Nordt et al., (2015), Kent et al. (2018), and Rasmussen et al. (2020)], and two age
732 models that are based on magnetostratigraphic and CA-TIMS geochronologic information (Kent et al.,
733 2019; Rasmussen et al., 2020). As shown on this figure, our LA-ICPMS MDA's reveal two first-order
734 patterns. The first pattern is that the LA-ICPMS-based MDA's overlap with most CA-TIMS ages and both
735 age models for most strata belonging to the Blue Mesa Member and Petrified Forest Member, but are

736 significantly older for strata of the Sonsela Member. The second pattern is that most LA-ICPMS-based
737 MDA's belong to three main clusters (~222-219 Ma, ~217-215 Ma, and ~212-211 Ma), whereas the other
738 chronologic records show a relatively simple pattern of upward younging (Fig. 13). The following
739 discussion explores these two patterns – details of the magnetostratigraphic information, CA-TIMS data,
740 and age models are discussed by Kent et al. (2018, 2019) and Rasmussen et al. (2020).

741 As shown on Figure 13, the LA-ICPMS-based MDA's presented herein overlap with the other
742 chronometers for sequences which are dominated by fine-grained strata (e.g., Blue Mesa Member and
743 Petrified Forest Member), but are several million years too old for sequences which are dominated by
744 coarse-grained strata (Sonsela Member) (Fig. 13). This pattern appears to hold for member-scale
745 stratigraphic units (e.g., strata from the Petrified Forest Member), although some individual samples
746 clearly do not follow this pattern. For example, of the six samples from the Petrified Forest Member that
747 yield maximum depositional ages which overlap with the other chronometers, four are mudstone-
748 siltstone and two are sandstone. In the lower Sonsela Member, of the six samples that yield maximum
749 depositional ages that predate the other chronometers, five are sandstone and one is siltstone. These
750 exceptions suggest that the dominant lithic characteristics and depositional environment of a member
751 (e.g., dominantly fine-grained floodplain deposits for the Petrified Forest Member versus dominantly
752 coarse-grained channel deposits of the Sonsela Member [Woody, 2006]), are more important than the
753 grain size of an individual horizon in controlling the recognition of near-depositional-age zircon grains.

754 The observed pattern that predominantly fine-grained strata of the Mesa Redondo, Blue Mesa, and
755 Petrified Forest members yield reliable MDA's, whereas predominantly coarse-grained sandstones of
756 the Sonsela Member do not, is surprising for two reasons. First, in terms of provenance (as described
757 above), strata of the Mesa Redondo, Blue Mesa, and Petrified Forest members are interpreted to have
758 been shed mainly from the Ouachita orogen, which lacks Triassic igneous rocks, whereas strata of the
759 Sonsela Member were shed from the Cordilleran magmatic arc to the southwest, which contains
760 abundant Permian and Triassic igneous rocks (Fig. 3). Second, as shown in the margins of Figures 7 and
761 8, Triassic zircon grains are significantly (~2x) more abundant in strata of the Sonsela Member than in
762 underlying and overlying strata. Based on these two observations, one might expect that strata of the
763 Sonsela Member would yield reliable MDA's, whereas strata from the Mesa Redondo Member, Blue
764 Mesa Member, and Petrified Forest Member would not.

765 We suggest that these counter-intuitive relations result in large part from our analytical method of only
766 analyzing zircon grains that are >60 um, combined with the maximum size of zircons that can be

767 transported in fine-grained versus coarse-grained sediments. For coarse-grained sediment, >60 um
768 zircon grains could include both transported (detrital) components that predate deposition, as well as
769 zircons that are air-fall in origin and approximately of depositional age. A MDA calculated from a mix of
770 these grains would accordingly pre-date deposition. In contrast, Triassic zircon grains from fine-grained
771 strata would tend to be mostly air-fall in origin given that the older, transported grains are too small to
772 analyze. A MDA calculated from zircons that are primarily of air-fall origin would accordingly approach
773 the true depositional age.

774 The relations described above suggest that convergence versus divergence of the chronologic records
775 results from connections between depositional setting, grain size, provenance, and analytical methods,
776 which together conspire to control the proportions of air-fall (near-depositional age) versus slightly
777 older detrital zircon grains recognized in our samples. We suggest that the three chronometric records
778 agree (to within ~1 m.y.) for strata of the lower Blue Mesa Member and middle-upper Petrified Forest
779 Member because of the availability of zircon grains of air-fall origin, which are near depositional age and
780 both <60 um and >60 um in size, versus the scarcity of pre-depositional-age Triassic grains of sufficient
781 size for analysis due to the lack of Triassic rocks in the source region (mainly the Ouachita orogen) and
782 the small (<60 um) grain size of most sediment. In contrast, for the Sonsela Member, the LA-ICPMS
783 MDA's are interpreted to pre-date the other chronologic records because the sediment was derived
784 from the south, where abundant igneous rocks of Permian-Triassic age were exposed, and the grain size
785 of the detrital (pre-depositional-age) zircons was sufficiently large that many would have been analyzed.

786 A test of this hypothesis is provided by MSWD values of the weighted means calculated for ages from
787 samples belonging to the various stratigraphic units. As shown in DR Table 6, average MSWD values for
788 samples from dominantly fine-grained strata of the Mesa Redondo-Blue Mesa and Petrified Forest units
789 are 1.7 and 1.3 (respectively), whereas coarser grained strata of the lower and upper Sonsela units yield
790 higher MSWD values of 2.6 and 2.1 (respectively). These values are consistent with the interpretation
791 that Triassic zircon grains in coarser-grained units have a greater range of ages than Triassic zircon grains
792 in finer-grained units.

793 These interpreted connections may also provide an explanation for the patterns of offset of the CA-TIMS
794 ages of Rasmussen et al. (2020) relative to the LA-ICPMS ages and magnetostratigraphic age models in
795 the Sonsela Member (Fig. 13). For strata of the upper Sonsela Member, the CA-TIMS and
796 magnetostratigraphic records converge because the methods of grain selection were apparently
797 successful in identifying populations of syn-depositional age zircon grains. For strata of the lower

798 Sonsela Member, however, these methods were unsuccessful in identifying a sufficient number of
799 depositional-age zircon grains to determine a reliable MDA, presumably because of their low abundance
800 relative to older transported grains.

801 The second main pattern exhibited by the three chronometers is that most of the LA-ICPMS-based
802 MDA's belong to three main clusters (~222-219 Ma, ~217-215 Ma, and ~212-211 Ma), whereas the other
803 chronologic records show a relatively simple pattern of upward younging (Fig. 13). For the ~222-219 Ma
804 cluster, a plausible interpretation, following from the connections described above, is that ~222-219 Ma
805 zircon grains of air-fall origin accumulated in fine-grained strata of the lower Blue Mesa Member, and
806 were then recycled from age-equivalent strata into predominantly coarser grained channel sands of the
807 upper Blue Mesa Member and lower Sonsela Member. Grains from these same sources appear to have
808 also been recycled into sandstone sample 131-2 of the lower Petrified Forest Member (Fig. 13). The
809 ~212-211 Ma cluster may have formed in a similar fashion, with initial accumulation of near-
810 depositional-age air-fall zircons in mudstones of sample 116-1, followed by recycling of these grains
811 from age-equivalent strata into coarser-grained strata of samples 104-3, 92-2, and 84-2 (Fig. 13).

812 The source of zircon grains that belong to the ~217-215 Ma cluster is less obvious given the lack of
813 recognized fine-grained strata dominated by zircons of this age (Fig. 13). One possibility is that ~217-215
814 Ma grains were eroded from fine-grained strata exposed elsewhere [perhaps near Sonsela Buttes
815 (Marsh et al., 2019) or near the Cordilleran magmatic arc] that are dominated by grains of this age. A
816 second possibility is that fine-grained strata dominated by ~217-215 Ma ages were originally present in
817 the lower Sonsela Member, but were removed by erosion and recycled into strata of the upper Sonsela
818 Member. Previous workers have suggested the existence of a hiatus or hiatuses (Ramezani et al., 2011)
819 or an erosional event (Rasmussen et al., 2020) at approximately this stratigraphic level, as shown by the
820 preferred age model of Rasmussen et al. (2020) on Figure 13. The occurrence of very different <240 Ma
821 ages, >240 Ma ages, and U/Th values in samples 196-3 and 195-2 suggests that this shift in provenance,
822 accumulation of a condensed section, or formation of an unconformity likely coincides with the
823 proposed boundary between strata of the lower Sonsela Member and upper Sonsela Member. As
824 discussed by Ramezani et al. (2011) and Rasmussen et al. (2020), the possibility of an unconformity or
825 condensed section near this stratigraphic position has important implications for Chinle stratigraphy and
826 fundamental Late Triassic biotic and climatic changes. It should be noted, however, that no stratigraphic
827 evidence for such an unconformity was recognized in the CPCP core.

828 10. IMPLICATIONS FOR THE STRATIGRAPHY OF THE CHINLE FORMATION

829 The interpreted connections between the three geochronologic records and Chinle stratigraphy
830 provide an opportunity to reconstruct the depositional history of the Chinle Formation.

831 Fundamental assumptions in reconstructing this history are that:

832 (1) Chinle Formation strata encountered in the CPCP core record nearly continuous deposition
833 as described in the age model of Kent et al. (2019), perhaps with a period of erosion or very
834 slow deposition in the middle part of the Sonsela Member (Rasmussen et al., ~~2019~~2020).

835 (2) LA-ICPMS ages recovered from strata of the Chinle Formation belong to five separate groups
836 (red vertical bars of Figure 13) due to the hypothesized connections between stratigraphy, grain
837 size, and proportions of near-depositional-age (air-fall) versus older (recycled) zircon ages.

838 (3) Late Triassic igneous activity in the Cordilleran magmatic arc provided a nearly continuous
839 supply of zircon grains of air-fall origin to the Chinle deposystem. This assumption is supported
840 by the relatively continuous distribution of U-Pb ages within the Cordilleran magmatic arc and
841 back-arc (upper curves of Figure 13). This view is in contrast to the hypothesis of Kent et al.
842 (2019) that variations in the proportions of depositional-age versus older zircon grains result
843 mainly from temporal changes in magmatic flux.

844 The interpreted stratigraphic evolution is summarized below and shown schematically on
845 Figure 14. Important phases in this evolution are as follows:

846 A: An LA-ICPMS MDA of ~223.3 Ma from our one sample from the Mesa Redondo Member
847 (305-2) agrees with the magnetostratigraphic information, the two age models, and the set of
848 CA-TIMS ages from this sample, presumably because these fine-grained strata are dominated
849 by zircon grains of air-fall origin. Older CA-TIMS ages of ~225.2 Ma (Ramezani et al., 2011) and
850 ~227.6 (Atchley et al., 2013) from outcrops of the Mesa Redondo Member may be
851 compromised by an abundance of recycled zircon grains.

852 B: LA-ICPMS ages of ~221 Ma from fine-grained strata in the lower part of the Blue Mesa
853 Member are also near depositional age, presumably because the >60 um zircon grains in these
854 fine-grained strata are dominated by air-fall (or slightly reworked) components.

855 C: LA-ICPMS ages from strata of the upper Blue Mesa Member significantly pre-date deposition,
856 presumably because these strata are dominated by recycled zircons. The predominance of ~221
857 Ma LA-ICPMS MDA's suggests that most zircon grains were recycled from lateral equivalents of
858 underlying strata in the lower part of the Blue Mesa Member. CA-TIMS ages also pre-date
859 deposition, presumably because of the difficulty of isolating near-depositional-age grains of air-
860 fall origin.

861 D: This pattern continues up through most of the lower Sonsela Member, with LA-ICPMS MDA's
862 remaining at ~221 due to recycling of strata from lateral equivalents of the lower Blue Mesa

863 Member. Most CA-TIMS ages predate the age of deposition because depositional-age (air fall)
864 grains were diluted by recycled components.

865 E: The age patterns from sandstones of the upper Sonsela Member are somewhat puzzling
866 given that the dominant ~217-215 Ma LA-ICPMS MDA's pre-date deposition, but fine-grained
867 strata that could have sourced grains of these ages are not present in the lower Sonsela
868 Member (Fig. 13). One possibility, as described above, is that the ~217-215 Ma grains were
869 eroded from fine-grained strata exposed elsewhere [~~(perhaps near Sonsela Buttes (Marsh et~~
870 ~~al., 2019)~~ [or from the Cordilleran magmatic arc](#)] that are dominated by grains of this age. A
871 second possibility is that fine-grained strata dominated by ~217-215 Ma ages were originally
872 present in the underlying lower Sonsela Member, but were removed by erosion and recycled
873 into strata of the upper Sonsela Member. An erosional event of the appropriate age and
874 stratigraphic position has been described by [Ramezani et al. \(2011\)](#) and by [Rasmussen et al.](#)
875 [\(2020\)](#), as shown by their age model on Figure 13. The occurrence of very different <240 Ma
876 ages, >240 Ma ages, and U/Th values in samples 196-3 and 195-2 suggests that this [change in](#)
877 [provenance, condensed section, or](#) unconformity most likely coincides with the boundary
878 between lower and upper Sonsela Member strata, ~~and perhaps with the red siliceous horizon~~
879 ~~recognized in the CPCP core.~~ As discussed by [Rasmussen et al. \(2020\)](#), the possibility of an
880 unconformity or condensed section near this stratigraphic position has important implications
881 for Chinle stratigraphy and fundamental Late Triassic biotic and climatic changes.

882 F: The dominance of pre-depositional-age grains in sample 131-2 provides strong evidence for
883 recycling of detrital zircons from lateral equivalents of underlying strata of the Blue Mesa
884 Member or lower Sonsela Member.

885 G: All chronometers agree for strata of sample 116-1, presumably because these fine-grained
886 strata are dominated by air-fall (or slightly reworked) detrital zircons.

887 H: LA-ICPMS MDA's from sandstones of the middle Petrified Forest Member (samples 104-3,
888 92-2, and 84-2) slightly predate deposition because they were recycled from lateral equivalents
889 of immediately underlying fine-grained strata (e.g., sample 116-1).

890 I: All chronometers agree for strata of the Black Forest bed because this unit is dominated by
891 air-fall (or slightly reworked) detrital zircon grains.

892 **11. CONCLUSIONS**

893 First-order conclusions that result from our U-Pb geochronologic analyses of detrital zircon
894 grains from the Coconino Sandstone, Moenkopi Formation, and Chinle Formation are as
895 follows:

896 1. The provenance of strata belonging to the Coconino Sandstone and Moenkopi Formation can
897 be reconstructed by comparison of our LA-ICPMS ages (Figures 5 and 6) with age distributions
898 that characterize potential source regions (Figure 3). As shown on Figures 5 and 11, data from
899 our sample of the Coconino Sandstone and equivalent sandstones of the southern Colorado

900 Plateau suggest that these strata belong to an eolian blanket that was derived largely from the
901 Ouachita and/or Appalachian orogens, whereas strata from the northern Colorado Plateau
902 consist mainly of sediment derived from local basement uplifts (Fig. 1; Dickinson and Gehrels,
903 2003; Gehrels et al., 2011; Lawton et al. (2015). Lower-Middle Triassic strata of the Moenkopi
904 Formation record a very different dispersal system, with most detritus derived from the
905 Ouachita orogen, the East Mexico arc, and early phases of the Cordilleran magmatic arc (Figures
906 6 and 9).

907 2. LA-ICPMS ages from strata of the Chinle Formation belong to five groups that generally
908 correspond to the main stratigraphic units (Figures 7, 8, and 13). Maximum depositional ages
909 calculated from <240 Ma ages and provenance interpretations derived from >240 Ma ages are
910 as follows:

911 -- Strata of the Mesa Redondo Member yield a preferred MDA of ~223.3 Ma, and were derived
912 mainly from the Ouachita orogen.

913 -- Strata of the Blue Mesa Member yield MDA's of ~220.7 to ~220.2 Ma, and were derived from
914 local basement and Ouachita sources.

915 -- Strata in the lower part of the Sonsela Member yield similar MDA's of ~220.9 to ~220.3 Ma
916 (plus an uppermost sample with an MDA of ~218.2 Ma). Detritus was derived mainly from local
917 basement (especially ~1.44 Ga) sources, perhaps located in the ancestral Mogollon highlands to
918 the south.

919 -- Strata in the upper part of the Sonsela Member yield younger MDA's of ~216.6 to ~215.1 Ma,
920 plus an uppermost sample with an MDA of ~213.8 Ma. Grains with >240 Ma ages were derived
921 mainly from Precambrian basement (mainly ~1.44 Ga) and Grenville-age rocks to south, as well
922 as the East Mexico arc.

923 -- Strata of the Petrified Forest Member yield ages that belong to three separate groups. The
924 lowest sample yields an MDA of ~221.5, which is significantly older than ages from adjacent
925 strata. The middle four samples yield MDA's of ~211.7 to ~211.2 Ma, whereas the upper two
926 samples yield MDA's of ~209.8 and ~209.6 Ma. All six upper samples contain abundant >240 Ma
927 grains that were shed from a broad range of Ouachita, local basement, and East Mexico arc
928 sources.

929 3. Patterns of U and Th concentration in Triassic zircon grains from the Chinle Formation belong
930 to four distinct groups that generally coincide with the chronostratigraphic units described
931 above. Changes in U and Th concentrations are interpreted to record variations in the chemistry
932 of arc magmatism through time, as has been documented previously by Barth and Wooden
933 (2006, 2011, 2013) and Riggs et al. (2010, 2012, 2016).

934 4. Comparison of the Chinle Formation MDA's with magnetostratigraphic information (Kent et
935 al., 2018, 2019) and CA-TIMS geochronologic information (Rasmussen et al., 2020~~19~~) from the
936 CPCP core, plus CA-TIMS ages reported from outcrop samples, indicates that LA-ICPMS MDA's

937 approximate depositional ages for most strata of the Mesa Redondo Member, Blue Mesa
938 Member, and Petrified Forest Member, but significantly pre-date deposition for strata of the
939 Sonsela Member (Fig. 13). The correlation of age patterns with stratigraphy is interpreted to
940 reflect the proportions of air-fall (or slightly reworked) versus recycled (older) zircon grains:
941 fine-grained strata are dominated by near-depositional ages because most zircon grains are air-
942 fall (or slightly reworked) in origin, whereas coarse-grained strata are dominated by pre-
943 depositional ages because recycled zircon grains dilute the abundance of air-fall crystals.

944 5. This hypothesized connection between stratigraphy and the three geochronologic records
945 supports the following depositional history for Chinle Formation strata encountered in the CPCP
946 core (Figures 13 and 14):

947 -- LA-ICPMS ages and magnetostratigraphic information (Kent et al., 2019) indicate that the
948 sampled part of the Mesa Redondo Formation was deposited at ~223.3 Ma. CA-TIMS ages of
949 ~225.2 Ma (Ramezani et al., 2011) and ~227.6 (Atchley et al., 2013) from outcrop samples
950 suggest that strata of the Mesa Redondo Member in other areas are dominated by older
951 recycled components.

952 -- Magnetostratigraphic information (Kent et al., 2019) suggests that strata of the Blue Mesa
953 Member and lower Sonsela Member accumulated between ~222 Ma and ~214 Ma, whereas
954 LA-ICPMS MDA's are consistently ~221 Ma for the same strata (except for the uppermost
955 sample of ~217 Ma). This suggests that most zircons in strata of the upper Blue Mesa Member
956 and lower Sonsela Member were recycled from lateral equivalents of strata of the lower Blue
957 Mesa Member. The observation that most CA-TIMS ages from these strata also pre-date
958 deposition is interpreted to result from the dilution of air-fall zircon crystals by older recycled
959 zircon grains.

960 -- Strata of the upper Sonsela Member accumulated between ~215 and ~213 Ma, as
961 constrained by magnetostratigraphic information and CA-TIMS ages. LA-ICPMS MDAs from
962 these strata are ~217-215 Ma, which indicates that they are dominated by zircons recycled
963 from older units. The lack of samples in the lower Sonsela Member that are dominated by
964 ~217-215 Ma grains suggests that zircon grains of this age in upper Sonsela Member strata may
965 have been transported from sections of the Chinle Formation exposed outside of the PEFO
966 area. It is also possible that such strata were exposed in the PEFO area, but were removed
967 during an erosional event inferred by Rasmussen et al. (2020~~19~~) from the pattern of CA-TIMS
968 ages in the upper Sonsela Member (Fig. 3). Significant changes in <240 Ma ages, >240 Ma ages,
969 and U-Th values suggest that this unconformity, if present, occurs between samples 196-3 and
970 195-2, ~~and may coincide with the red siliceous horizon recognized in the CPCP core.~~

971 -- All available evidence suggests that mudstone and subordinate sandstone of the middle
972 Petrified Forest Member accumulated at ~212-211 Ma, and the Black Forest bed in the upper
973 part of the unit accumulated at ~210 Ma. In contrast, LA-ICPMS ages recovered from sample
974 131-2, from the lower part of the Petrified Forest Member, are dominantly ~221 Ma, suggestive

975 of recycling from lateral equivalents of strata of the Blue Mesa Member and lower Sonsela
976 Member.

977 6. Comparisons of our LA-ICPMS ages, the available CA-TIMS data, and magnetostratigraphic
978 information provide insights into methods for determining the depositional age of fluvial strata.
979 Our results show that the most reliable information comes from sequences dominated by fine-grained
980 clastic strata (mudstone and siltstone) given that these strata have a low abundance of pre-depositional-
981 age zircon grains of the appropriate size (>60 μm diameter) for routine analysis by LA-ICPMS. Mudstone-
982 siltstone samples may accordingly ~~yield have~~ a high proportion of >60 μm zircon grains that are air-fall in
983 origin (or only slightly reworked) and thereby record the age of deposition. In contrast, sedimentary
984 sequences dominated by sandstone ~~could well commonly~~ yield abundant >60 μm zircon grains that
985 ~~predate deposition have been recycled from older sediments~~, thereby diluting syn-depositional-age
986 zircon grains. Future attempts to determine depositional ages from fluvial strata should accordingly
987 focus on sequences dominated by fine-grained strata, rather than sandstones, in spite of the challenges
988 of extracting and analyzing the smaller zircon crystals.

989 **12. AUTHOR CONTRIBUTION**

990 NG and GG generated the LA-ICPMS data reported in this paper. All coauthors were involved in
991 acquiring the samples that were analyzed and/or interpreting the data. GG prepared this
992 manuscript with input from all co-authors.

993 **13. COMPETING INTERESTS**

994 The authors declare that they have no conflict of interest.

995 **14. ACKNOWLEDGEMENTS**

996 Geochronologic analyses were conducted with support from NSF EAR-0959107 and EAR-
997 1649254 (to Gehrels). Laboratory analyses were performed primarily by N. Giesler.
998 Collaborative aspects of the project were supported by NSF EAR 0958976 (PEO & JWG),
999 0958723 (RM), 0958915 (RBI), and 0958859 (DVK). Funding for coring and much logistical
1000 support was provided by ICDP (International Scientific Continental Drilling Program grant 05-
1001 2010: JWG, PEO, Jingeng Sha, Roberto Molina-Garza, Wolfram Kürschner, and Gerhard
1002 Bachmann). Additional funding was supplied by grants from the Lamont Climate Center (PEO).
1003 Field support was provided by LacCore personnel (Anders Noren, Kristina Brady, and Ryan
1004 O'Grady), drilling manager Doug Schnurrenberger, and core-handling volunteers (Justin Clifton,
1005 Bob Graves, Ed Lamb, Max Schnurrenberger, and Riley Black). Superintendent Brad Traver of
1006 the National Park Service arranged for permission to core in the PEFO and provided logistical
1007 support during site selection and drilling. This is Petrified Forest Paleontological Contribution 67.
1008 The conclusions presented here are those of the authors and do not represent the views of the
1009 United States Government.

1010 **REFERENCES CITED**

- 1011 Alsalem, O.B., Fan, M., Zamora, J., Xie, X., and Griffin, W.R.: Paleozoic sediment dispersal before
1012 and during the collision between Laurentia and Gondwana in the Fort Worth Basin, USA:
1013 *Geosphere*, v. 14, no. 1, p. 1–18, doi: 10.1130/GES01480.1, 2018.
- 1014 Ash, S.R.: The Black Forest Bed, a distinctive unit in the Upper Triassic Chinle Formation, north-
1015 eastern Arizona: *Journal of the Arizona-Nevada Academy of Science*, v. 24–25, p. 59–73, 1992.
- 1016 Atchley, S.C., Nordt, L.C., Dworkin, S.I., Ramezani, J., Parker, W.G., Ash, S.R., and Bowring, S.A.:
1017 A linkage among Pangean tectonism, cyclic alluviation, climate change, and biologic turnover in
1018 the Late Triassic: The Record from the Chinle Formation, Southwestern United States: *Journal of*
1019 *Sedimentary Research*, v. 83, p. 1147–1161, 2013.
- 1020 Baranyi, V., Reichgelt, T., Olsen, P.E., Parker, W.G., Kürschner, W.M.: Norian vegetation history
1021 and related environmental changes: new data from the Chinle Formation, Petrified Forest
1022 National Park (Arizona, SW USA): *Geological Society of America Bulletin*, v. 130, p. 775–795,
1023 doi.org/10.1130/B31673.1, 2017.
- 1024 Barth, A.P. and Wooden, J.L.: Timing of magmatism following initial convergence at a passive
1025 margin, southwestern US Cordillera, and ages of lower crustal magma sources: *Journal of*
1026 *Geology*, v. 114, p. 231–245, 2006.
- 1027 Barth, A.P., Walker, J.D., Wooden, J.L., Riggs, N.R., and Schweickert, R.A.: Birth of the Sierra
1028 Nevada magmatic arc: Early Mesozoic plutonism and volcanism in the east-central Sierra
1029 Nevada of California: *Geosphere*, v. 7, p. 877–897, 2011.
- 1030 Barth, A.P., Wooden, J.L., Jacobson, C.E., and Economos, R.C.: Detrital zircon as a proxy for
1031 tracking the magmatic arc system: The California arc example: *Geology*, v. 41, p. 223–226, 2013.
- 1032 Black, L., Kamo, S., Allen, C., Davis, D., Aleinikoff, J., Valley, J., Mundil, R., Campbell, I., Korsch,
1033 R., Williams, I., and Foudoulis, C.: Improved $^{206}\text{Pb}/^{238}\text{U}$ microprobe geochronology by the
1034 monitoring of a trace-element-related matrix effect; SHRIMP, ID-TIMS, ELA-ICP-MS and
1035 oxygen isotope documentation for a series of zircon standards: *Chemical Geology*, v. 205, p.
1036 115–140, 2004.
- 1037 Blakey, R.C., Peterson, F., and Kocurek, G.: Synthesis of late Paleozoic and Mesozoic eolian
1038 deposits of the western interior of the United States: *Sedimentary Geology*, v. 56, p. 3–125,
1039 1988.
- 1040 Chen, J.H., and Moore, J.G.: Uranium-lead isotopic ages from the Sierra Nevada batholith:
1041 *Journal of Geophysical Research*, v. 87, p. 4761–4784, 1982.
- 1042 Cohen, K.M., Finney, S.C., Gibbard, P.L., and Fan, J.-X.: The ICS International Chronostratigraphic
1043 Chart: Episodes v. 36, p. 199–204 (updated 2018), 2013.

- 1044 Creber, G.T., and Ash, S.R.: Evidence of widespread fungal attack on Upper Triassic trees in the
1045 southwestern U.S.A.: *Review of Palaeobotany and Palynology*, v. 63, p. 189-195, 1990.
- 1046 DeGraaff-Surples, K., Graham, S.A., Wooden, J.L., and McWilliams, M.O.: Detrital zircon
1047 provenance analysis of the Great Valley Group, California: Evolution of an arc-forearc system:
1048 *Geological Society of America Bulletin*, v. 114 (12), p. 1564–1580, 2002.
- 1049 Dickinson, W.R.: Tectonosedimentary Relations of Pennsylvanian to Jurassic strata on the
1050 Colorado Plateau, *Geological Society of America Special Paper 533*, 184 p., 2018.
- 1051 Dickinson, W.R., and Gehrels, G.E.: U-Pb ages of detrital zircon grains from Permian and Jurassic
1052 eolian sandstones of the Colorado Plateau, USA: Paleogeographic implications: *Sedimentary
1053 Geology*, v. 163, p. 29–66, 2003.
- 1054 Dickinson, W.R. and Gehrels, G.E.: U-Pb ages of detrital zircon grains in relation to
1055 paleogeography: Triassic paleodrainage networks and sediment dispersal across southwest
1056 Laurentia: *Journal of Sedimentary Research*, v. 78, p. 745–764, 2008.
- 1057 Dickinson, W.R. and Gehrels, G.E.: Use of U–Pb ages of detrital zircon grains to infer maximum
1058 depositional ages of strata: a test against a Colorado Plateau Mesozoic database: *Earth and
1059 Planetary Science Letters*, v. 288, p. 115–125, 2009.
- 1060 Gehrels, G.E.: Introduction to detrital zircon studies of Paleozoic and Triassic strata in western
1061 Nevada and northern California, in Soreghan, M.J. and Gehrels, G.E., eds., *Paleozoic and Triassic
1062 paleogeography and tectonics of western Nevada and northern California: Geological Society of
1063 America Special Paper 347*, p. 1-18, 2000.
- 1064 Gehrels, G.E.: Detrital zircon U-Pb geochronology applied to tectonics: *Annual Review of Earth
1065 and Planetary Sciences*, v. 42, p. 127-149, 2014.
- 1066 Gehrels, G. and Pecha, M.: Detrital zircon U-Pb geochronology and Hf isotope geochemistry of
1067 Paleozoic and Triassic passive margin strata of western North America: *Geosphere*, v. 10 (1), p.
1068 49-65, 2014.
- 1069 Gehrels, G.E., Valencia, V., Pullen, A.: Detrital zircon geochronology by Laser-Ablation
1070 Multicollector ICPMS at the Arizona LaserChron Center, in Loszewski, T., and Huff, W., eds.,
1071 *Geochronology: Emerging Opportunities*, *Paleontology Society Short Course: Paleontology
1072 Society Papers*, v. 11, 10 p., 2006.
- 1073 Gehrels, G.E., Valencia, V., Ruiz, J.: Enhanced precision, accuracy, efficiency, and spatial
1074 resolution of U-Pb ages by laser ablation–multicollector–inductively coupled plasma–mass
1075 spectrometry: *Geochemistry, Geophysics, Geosystems*, v. 9, Q03017,
1076 doi:10.1029/2007GC001805, 2008.

- 1077 Gehrels, G., Blakey, R., Karlstrom, K., Timmons, M., Dickinson, W., and Pecha, M.: Detrital zircon
1078 U-Pb geochronology of Paleozoic strata in the Grand Canyon: *Lithosphere*, v. 3 (3), p. 183-200,
1079 2011.
- 1080 González-León, C.M., Valencia, V.A., Lawton, T.F., Amato, J.M., Gehrels, G.E., Leggett, W.J.,
1081 Montijo-Contreras, O., Fernández, M.A.: The lower Mesozoic record of detrital zircon U-Pb
1082 geochronology of Sonora, México, and its paleogeographic implications: *Revista Mexicana de*
1083 *Ciencias Geológicas*, v. 26 (2), p. 301-314, 2009.
- 1084 Heckert, A.B. and Lucas, S.G.: Revised Upper Triassic stratigraphy of the Petrified Forest
1085 National Park, Arizona, USA: *New Mexico Museum of Natural History Science Bulletin*, v. 21, p.
1086 1–36, 2002.
- 1087 Heckert, A.B., Lucas, S.G., Dickinson, W.R., and Mortensen, J.K.: New ID-TIMS U-Pb ages for
1088 Chinle Group strata (Upper Triassic) in New Mexico and Arizona, correlation to the Newark
1089 Supergroup, and implications for the “long Norian”: *Geological Society of America Abstracts*
1090 *with Programs*, v. 41, p. 123, 2009.
- 1091 Hildebrand, R.S.: Did westward subduction cause Cretaceous-Tertiary orogeny in the North
1092 American Cordillera?: *Geological Society of America Special paper* 457, 71 p., 2009.
- 1093 Hildebrand, R.S.: Mesozoic assembly of the North American cordillera: *Geological Society of*
1094 *America Special paper* 495, 169 p., 2013.
- 1095 Hoke, G., Schmitz, M., and Bowring, S.: An ultrasonic method for isolating nonclay components
1096 from clay-rich material: *Geochemistry Geophysics Geosystems*, v. 15, p. 492–498, 2014.
- 1097 Horstwood, M., Kosler, J., Gehrels, G., Jackson, S., McLean, N., Paton, C., Pearson, N., Sircombe,
1098 K., Sylvester, P., Vermeesch, P., Bowring, J., Condon, D., and Schoene, B.: Community-Derived
1099 Standards for LA-ICP-MS U-Th-Pb Geochronology – Uncertainty Propagation, Age Interpretation
1100 and Data Reporting: *Geostandards and Geoanalytical Research*, v. 40 (3), p. 311-332, 2016.
- 1101 Irmis, R.B., Mundil, R., Martz, J.W., and Parker, W.G.: High-resolution U-Pb ages from the Upper
1102 Triassic Chinle Formation (New Mexico, USA) support a diachronous rise of dinosaurs: *Earth and*
1103 *Planetary Science Letters*, v. 309, p. 258–267, 2011.
- 1104 Kent, D.V., Olsen, P.E., and Muttoni, G.: Astrochronostratigraphic polarity time scale (APTS) for
1105 the Late Triassic and Early Jurassic from continental sediments and correlation with standard
1106 marine stages: *Earth-Science Reviews*, v. 166, p. 153–180, 2017.
- 1107 Kent, D.V., Olsen, P.E., Rasmussen, C., Lepre, C.J., Mundil, R., Irmis, R.B., Gehrels, G.E., Giesler,
1108 D., Geissman, J.W., and Parker, W.G.: Empirical evidence for stability of the 405 kyr Jupiter-
1109 Venus eccentricity cycle over hundreds of millions of years: *Proceedings of the National*
1110 *Academy of Sciences*, v. 115, p. 6153–6158, 2018.

- 1111 Kent, D.V., Olsen, P.E., Lepre, C. Mundil, R., Rasmussen, C., Irmis, R.B., Gehrels, G.E., Giesler, D.,
1112 Geissman, J.W., Parker, W.G.: Magnetostratigraphy of the entire Chinle Formation (Norian age)
1113 in scientific drill core PFNP-1A from the Petrified Forest National Park (Arizona, USA) and
1114 implications for global correlations in the Late Triassic: *Geophysics, Geochemistry, Geosystems*
1115 (in review), 2019.
- 1116 Kissock, J.K., Finzel, E.S., Malone, D.H., and Craddock, J.P.: Lower–Middle Pennsylvanian strata
1117 in the North American midcontinent record the interplay between erosional unroofing of the
1118 Appalachians and eustatic sea-level rise: *Geosphere*, v. 14 (1), p. 141–161, 2018.
- 1119 Lawton, T.F., Buller, C.D., and Parr, T.R.: Provenance of a Permian erg on the western margin of
1120 Pangea: Depositional system of the Kungurian (late Leonardian) Castle Valley and White Rim
1121 sandstones and subjacent Cutler Group, Paradox Basin, Utah, USA: *Geosphere*, v. 11 (5), p. 1–
1122 32, 2015.
- 1123 Lucas, S.G.: The Chinle Group: revised stratigraphy and biostratigraphy of Upper Triassic
1124 nonmarine strata in the western United States, in: *Aspects of Mesozoic Geology and*
1125 *Paleontology of the Colorado Plateau*, edited by: Morales, M., Museum of Northern Arizona
1126 Bulletin 59, Flagstaff: Museum of Northern Arizona Press, p. 27–50., 1993.
- 1127 Ludwig, K.R.: Isoplot 3.6: Berkeley Geochronology Center Special Publication 4, 77 p., 2008.
- 1128 Marsh, A.D., Parker, W.G., Stockli, D.F., and Martz, J.W.: Regional correlation of the Sonsela
1129 Member (Upper Triassic Chinle Formation) and detrital U-Pb zircon data from the Sonsela
1130 Sandstone bed near the Sonsela Buttes, northeastern Arizona, USA, support the presence of a
1131 distributive fluvial system: *Geosphere*, v. 15, <https://doi.org/10.1130/GES02004.1>, 2019.
- 1132 Martz, J.W. and Parker, W.G.: Revised lithostratigraphy of the Sonsela Member (Chinle
1133 Formation, Upper Triassic) in the southwestern part of Petrified Forest National Park, Arizona:
1134 *PLoS ONE* 5(2): e9329. doi:10.1371/journal.pone.0009329, 2010.
- 1135 Martz, J.W., Parker, W.G., Skinner, L., Raucchi, J.J., Umhoefer, P., and Blakey, R.C.: Geologic map
1136 of Petrified Forest National Park, Arizona: Arizona Geological Survey Contributed Map CM-12-A,
1137 1 map sheet, scale 1:50,000, 18 p., http://repository.azgs.gov/uri_gin/azgs/dlio/1487, 2012.
- 1138 Martz, J.W., Kirkland, J.I., Milner, A.R.C., Parker, W.G., Santucci, V.L.: Upper Triassic
1139 lithostratigraphy, depositional systems, and vertebrate paleontology across southern Utah:
1140 *Geology of the Intermountain West*, v. 4, p. 99-180, [https://www.utahgeology.org/wp-](https://www.utahgeology.org/wp-content/uploads/2018/05/GIW2017-v04-pp099-180-Martz.pdf)
1141 [content/uploads/2018/05/GIW2017-v04-pp099-180-Martz.pdf](https://www.utahgeology.org/wp-content/uploads/2018/05/GIW2017-v04-pp099-180-Martz.pdf), 2017.
- 1142 Miller, J.S., Glazner, A.F., Walker, J.D., and Martin, M.W.: Geochronologic and isotopic evidence
1143 for Triassic–Jurassic emplacement of the eugeoclinal allochthon in the Mojave Desert region,
1144 California: *Geological Society of America Bulletin*, v. 107, p. 1441–1457, 1995.

- 1145 Nordt, L., Atchley, S., Dworkin, S.: Collapse of the Late Triassic megamonsoon in western
1146 equatorial Pangea, present-day American southwest: *Geological Society of America Bulletin*, v.
1147 127 (11/12), p. 1798–1815, 2015.
- 1148 Olsen, P. E., Kent, D.V., and Whiteside, H.: Implications of the Newark Supergroup-based
1149 astrochronology and geomagnetic polarity time scale (Newark-APTS) for the tempo and mode
1150 of the early diversification of the Dinosauria: *Earth and Environmental Science Transactions of*
1151 *the Royal Society of Edinburgh*, v. 101, p. 201–229, 2011.
- 1152 Olsen, P., Geissman, J., Kent, D., Gehrels, G., and 23 others: Colorado Plateau Coring Project,
1153 Phase I (CPCP-I): a continuously cored, globally exportable chronology of Triassic continental
1154 environmental change from western North America: *Scientific Drilling*, v. 24, p. 15–40, 2018.
- 1155 Olsen, P.E., Laskar, J., Kent, D.V., Kinney, S.T., Reynolds, D.J., Sha, J. and Whiteside, J.H.:
1156 Mapping Solar System chaos with the Geological Orrery: *Proceedings of the National Academy*
1157 *of Sciences*, v. 116 (22), p. 10664-10673, 2019.
- 1158 Ortega-Flores, B., Solari, L., Lawton, T.F., and Ortega-Obregón, C.: Detrital-zircon record of
1159 major Middle Triassic–Early Cretaceous provenance shift, central Mexico: demise of
1160 Gondwanan continental fluvial systems and onset of backarc volcanism and sedimentation:
1161 *International Geology Review*, v. 56 (2), p. 237-261, 2014.
- 1162 Paces, J.B., & Miller, J.D.: Precise U-Pb ages of Duluth Complex and related mafic intrusions,
1163 northeastern Minnesota: Geochronological insights to physical, petrogenetic, paleomagnetic,
1164 and tectonomagmatic processes associated with the 1.1 Ga midcontinent rift system: *Journal of*
1165 *Geophysical Research*, v. 98 (B8), p. 13997–14013. <https://doi.org/10.1029/93JB01159>, 1993.
- 1166 Parker, W., and Martz, J.: Constraining the stratigraphic position of the Late Triassic (Norian)
1167 Adamanian-Revueltian faunal transition in the Chinle Formation of Petrified Forest National
1168 Park, Arizona: *Journal of Vertebrate Paleontology*, v. 29 (suppl. to 3), p. 162A, 2009.
- 1169 Parker, W.G., and Martz, J.W.: The Late Triassic (Norian) Adamanian–Revueltian tetrapod faunal
1170 transition in the Chinle Formation of Petrified Forest National Park, Arizona, *Earth and*
1171 *Environmental Science Transactions of the Royal Society of Edinburgh*: v. 101, p. 231–260,
1172 2011.
- 1173 Pipiringos, G.N., O’Sullivan, R.B.: Principal unconformities in Triassic and Jurassic rocks, Western
1174 Interior United States – a preliminary survey: *Geological Survey Professional Paper 1035-A*, 29
1175 p., 1978.
- 1176 Pullen, A., Ibanez-Mejia, M., Gehrels, G., Giesler, D., and Pecha, M.: Optimization of a Laser
1177 Ablation-Single Collector-Inductively Coupled Plasma-Mass Spectrometer (Thermo Element 2)
1178 for Accurate, Precise, and Efficient Zircon U-Th-Pb Geochronology: *Geochemistry, Geophysics,*
1179 *Geosystems*, v. 19. <https://doi.org/10.1029/2018GC007889>, 2018.

1180 Ramezani, J., Hoke, G.D., Fastovsky, D.E., Bowring, S.A., Therrien, F., Dworkin, S.I., Atchley, S.C.,
1181 and Nordt, L.C.: High precision U-Pb zircon geochronology of the Late Triassic Chinle Formation,
1182 Petrified Forest National Park (Arizona, USA): Temporal constraints on the early evolution of
1183 dinosaurs: *Geological Society of America Bulletin*, v. 123, p. 2142–2159, 2011.

1184 Ramezani, J., Fastovsky, D.E., and Bowring, S.A.: Revised chronostratigraphy of the lower Chinle
1185 Formation strata in Arizona Arizona and New Mexico (USA): high-precision U-Pb
1186 geochronological constraints on the Late Triassic evolution of dinosaurs: *American Journal of
1187 Science*, v. 314, p. 981–1008, 2014.

1188 Rasmussen, C., Mundil, R., Irmis, R.B., Geisler, D., Gehrels, G.E., Olsen, P.E., Kent, D.V., Lepre, C.,
1189 Geissmann, J.W., and Parker, W.G.: A high-resolution age model for the Upper Triassic Chinle
1190 Formation (Petrified Forest National Park, Arizona, USA) constrained by U-Pb geochronology
1191 and magnetostratigraphy: implications for Late Triassic paleoecological and
1192 paleoenvironmental change: *Geological Society of America Bulletin* (in review), 202019.

1193 Reichgelt, T., Parker, W.G., Martz, J.W., Conran, J.G., Cittert, J.H.A.K., Kürschner, W.M.: The
1194 palynology of the Sonsela Member (Late Triassic, Norian) at Petrified Forest National Park,
1195 Arizona, USA: *Review of Palaeobotany and Palynology*, v. 189, p. 18-28,
1196 doi.org/10.1016/j.revpalbo.2012.11.001, 2013.

1197 Riggs, N.R., Lehman, T.M., Gehrels, G.E., and Dickinson, W.R.: Detrital zircon link between
1198 headwaters and terminus of the Upper Triassic Chinle–Dockum paleoriver system: *Science*, v.
1199 273, p. 97–100, 1996.

1200 Riggs, N.R., Ash, S.R., Barth, A.P., Gehrels, G.E., and Wooden, J.L.: Isotopic age of the Black
1201 Forest Bed, Petrified Forest Member, Chinle Formation, Arizona: an example of dating a
1202 continental sandstone: *Geological Society of America Bulletin*, v. 115, p. 1315–1323, 2003.

1203 Riggs, N.R., Barth, A.P., González-León, C., Jacobson, C.E., Howell, E., Wooden, J.E., and Walker,
1204 J.D.: Provenance of Upper Triassic strata in southwestern North America as suggested by
1205 isotopic analysis and chemistry of zircon crystals, in Rasbury, E.T., Hemming, S., and Riggs, N.,
1206 eds., *Mineralogical and Geochemical Approaches to Provenance: Geological Society of America
1207 Special Paper 487*, p. 13–36, doi: 10.1130 /2012 .2487 (02), 2012.

1208 Riggs, N.R., Reynolds, S.J., Lindner, P.J., Howell, E.R., Barth, A.P., Parker, W.G., and Walker, J.D.:
1209 The Early Mesozoic Cordilleran arc and Late Triassic paleotopography: The detrital record in
1210 Upper Triassic sedimentary successions on and off the Colorado Plateau: *Geosphere*, v. 9, p.
1211 602–613, 2013.

1212 Riggs, N.R., Oberling, Z.A., Howell, E.R., Parker, W.G., Barth, A.P., Cecil, M.R., and Martz, J.W.:
1213 Sources of volcanic detritus in the basal Chinle Formation, southwestern Laurentia, and
1214 implications for the Early Mesozoic magmatic arc: *Geosphere*, v. 12, p. 439–463, 2016.

- 1215 Saleeby, J., and Dunne, G.: Temporal and tectonic relations of early Mesozoic arc magmatism,
1216 southern Sierra Nevada, California, in Anderson, T.H., Didenko, A.N., Johnson, C.L., Khanchuk,
1217 A.I., and MacDonald, J.H., Jr., eds., Late Jurassic Margin of Laurasia—A Record of Faulting
1218 Accommodating Plate Rotation: Geological Society of America Special Paper 513, p. 223–268,
1219 2015.
- 1220 Saylor, J.E., and Sundell, K.E.: Quantifying comparison of large detrital geochronology data sets.
1221 *Geosphere*12, 203–220, 2016.
- 1222 Saylor, J.E., Jordan, J.C., Sundell, K.E., Wang, X., Wang, S., and Deng, T.: Topographic growth of
1223 the Jishi Shan and its impact on basin and hydrology evolution, NE Tibetan Plateau: *Basin*
1224 *Research*, v. 30(3), p. 544-563, 2018.
- 1225 Stewart, J.H., Anderson, T.H., Haxel, G.B., Silver, L.T., and Wright, J.E.: Late Triassic
1226 paleogeography of the southern Cordillera: The problem of a source for the voluminous
1227 volcanic detritus in the Chinle Formation of the Colorado Plateau region: *Geology*, v. 14, p. 567–
1228 570, 1986.
- 1229 Sundell, K.E., Saylor, J.E., and Pecha, M.: Sediment provenance and recycling of detrital zircons
1230 from Cenozoic Altiplano strata in southern Peru and implications for the crustal evolution of
1231 west-central South America: *Journal of South American Earth Sciences*, (in review), 2019.
- 1232 Surpless, K.D., Graham, S.A., Covault, J.A., and Wooden, J.L.: Does the Great Valley Group
1233 contain Jurassic strata? Reevaluation of the age and early evolution of a classic forearc basin:
1234 *Geology*, v. 34 (1), p. 21–24, 2006.
- 1235 Thomas, W.A., Gehrels, G.E., Greb, S.F., Nadon, G.C., Satkoski, A.M., and Romero, M.C.: Detrital
1236 zircon grains and sediment dispersal in the Appalachian foreland: *Geosphere*, v. 13 (6), p. 2206-
1237 2230, 2017.
- 1238 Thomas, W.A., Gehrels, G.E., Lawton, T., Satterfield, J., Romero, M., and Sundell, K.: Detrital
1239 zircon grains and sediment dispersal from the Coahuila terrane of northern Mexico into the
1240 Marathon foreland of the southern Midcontinent: *Geosphere*, v. 16 (in press), 2019.
- 1241 Tobisch, O.T., Fiske, R.S., Saleeby, J.B., Holt, E., and Sorensen, S.S.: Steep tilting of metavolcanic
1242 rocks by multiple mechanisms, central Sierra Nevada, California: *Geological Society of America*
1243 *Bulletin*, v. 112 (7), p. 1043–1058, 2000.
- 1244 Vermeesch, P.: Multi-sample comparison of detrital age distributions: *Chemical Geology*, v. 341,
1245 p. 140-146, 2013.
- 1246 [Vermeesch, P.: Dissimilarity measures in detrital geochronology: *Earth-Science Reviews*, v.](#)
1247 [178: p. 310–321, 2018a. doi: 10.1016/j.earscirev.2017.11.027.](#)
- 1248 [Vermeesch, P.: Statistics for fission tracks. In Malus'á, M. and Fitzgerald, P., editors, *Fission*](#)

- 1249 [track thermochronology and its application to geology. Springer, 2018b.](#)
- 1250 Wissink, G.K., Wilkinson, B.H., and Hoke, G.D.: Pairwise sample comparisons and
1251 multidimensional scaling of detrital zircon ages with examples from the North American
1252 platform, basin, and passive margin settings: *Lithosphere*, <https://doi.org/10.1130/L700.1>,
1253 2018.
- 1254 Woody, D.T.: Revised stratigraphy of the lower Chinle Formation (Upper Triassic) of Petrified
1255 Forest National Park, Arizona: *Museum of Northern Arizona Bulletin*, v. 62, p. 17–45, 2006.
- 1256 Wright, J.E., and Wyld, S.J.: Alternative tectonic model for Late Jurassic through Early
1257 Cretaceous evolution of the Great Valley Group, California, in Cloos, M., Carlson, W.D., Gilbert,
1258 M.C., Liou, J.G., and Sorensen, S.S., eds., *Convergent Margin Terranes and Associated Regions:
1259 A Tribute to W.G. Ernst: Geological Society of America Special Paper 419*, p. 1-15, 2007.
- 1260 Xie, X., Anthony, J.M., and Busbey, A.B.: Provenance of Permian Delaware Mountain Group,
1261 central and southern Delaware basin, and implications of sediment dispersal pathway near the
1262 southwestern terminus of Pangea: *International Geology Review*, DOI:
1263 10.1080/00206814.2018.1425925, 2018.

1264 **FIGURE CAPTIONS**

1265 **Figure 1.** Map showing the main basement provinces of southern North America and Mexico.
1266 Also shown are locations of the study area within the Colorado Plateau, outlines of Ancestral
1267 Rocky Mountains uplifts, and the Permian-Triassic magmatic arc along the continental margin
1268 of southwestern North America. Modified from Gehrels et al. (2011).

1269 **Figure 2.** Strata encountered in the Colorado Plateau Coring Project (adapted from Olsen et al.,
1270 2018). Sampled horizons are shown relative to core depth, stratigraphic depth, and
1271 stratigraphic nomenclature relevant for the Petrified Forest region. Detailed descriptions of
1272 samples are provided in DR Table 1; images of the sampled material are presented in Appendix
1273 1.

1274 **Figure 3.** Normalized probability density plots of U-Pb (zircon) ages from source terranes.
1275 Distinctive age groups include 1750-1620 Ma and 1520-1360 Ma ages from southwest Laurentia
1276 basement provinces, 1240-960 Ma ages from Grenville-age provinces exposed in the
1277 Appalachian and Ouachita orogens, 640-570 Ma and 480-370 Ma ages characteristic of the
1278 Appalachian orogen, 670-300 Ma ages from the Ouachita orogen, 300-260 Ma ages from the
1279 East Mexico arc, and 260-200 Ma ages belonging to the Cordilleran magmatic arc of
1280 southwestern North America. See text for sources of information.

1281 **Figure 4.** Plot showing the accuracy of $^{206}\text{Pb}^*/^{238}\text{U}$ dates of secondary standards analyzed
1282 during the current study. Each pair of symbols represents the weighted mean age and 2σ
1283 uncertainty of R33 and FC-1 analyses conducted with each sample, expressed as % offset from
1284 reported ID-TIMS dates of 1099.9 Ma for FC-1 (Paces and Miller, 1993) and 419.26 Ma for R33
1285 (Black et al., 2004). For FC-1, 1065 analyses are reported, with MSWD = 0.95 for all analyses. For
1286 R33, 295 analyses are reported, with MSWD = 0.92 for all analyses. Data are reported in DR
1287 Table 7.

1288 **Figure 5.** Normalized probability density plots of detrital zircon ages from our sample of the
1289 Coconino Sandstone and from other lower Permian sandstones of the Colorado Plateau.
1290 Numbers of constituent analyses are shown for each sample. Data are from ¹Dickinson and
1291 Gehrels (2003), ²Gehrels et al. (2011), ³Lawton et al. (2015), and ⁴this study. Shown for
1292 reference are age ranges from the Appalachian orogen (purple bands) and from local basement
1293 rocks (blue bands) (from Figure 3), which are interpreted by previous researchers to have
1294 sourced most of the detritus in these units. Also shown is our sample 383-2, which is
1295 interpreted to belong to the Wupatki Member of the Moenkopi Formation, but has an age
1296 signature characteristic of lower Permian strata of the Colorado Plateau.

1297 **Figure 6.** Probability density plots of detrital zircon ages from four samples from the Moenkopi
1298 Formation (lower four curves) as well as a Moenkopi sample from Dickinson and Gehrels
1299 (2008). Numbers of constituent analyses are shown for each sample. Samples 349-3, 335-1,
1300 327-2, and 319-2, plus the sample from Dickinson and Gehrels (2008), are all from the Holbrook

1301 Member. Sample 383-2 is interpreted to belong to the Wupatki Member, but has an age
1302 distribution that resembles lower Permian strata. Source regions are interpreted to include
1303 local basement rocks (blue bands), the Ouachita orogen (green bands), the East Mexico arc (red
1304 band), and the Late Permian-Triassic arc built along the Cordilleran margin (orange band).

1305 **Figure 7.** Normalized probability density plots of detrital zircon ages from twenty-four samples
1306 from the Mesa Redondo, Blue Mesa, Sonsela, and Petrified Forest Members of the Chinle
1307 Formation. Numbers of constituent analyses are shown for each sample. Age distributions older
1308 than 240 Ma are exaggerated by 10x. Tick marks indicate the preferred maximum depositional
1309 age for each sample (from DR Table 6). Source regions are interpreted to include local
1310 basement rocks (blue bands), the Ouachita orogen (green bands), the East Mexico arc (red
1311 band), and the Late Permian-Triassic arc built along the Cordilleran margin (orange band).
1312 Percent of all grains that are <240 Ma in age are shown for each sample on the left.

1313 **Figure 8.** Normalized probability density plots of detrital zircon ages from each set of samples
1314 analyzed in this study. Numbers of constituent analyses are shown for each sample. Age
1315 distributions older than 240 Ma for Chinle strata are exaggerated by 10x relative to <240 Ma
1316 ages. Age distributions for Moenkopi and Coconino Sandstones are exaggerated by 5x relative
1317 to Chinle ages. Source regions are interpreted to include local basement rocks (blue bands), the
1318 Ouachita orogen (green bands), the East Mexico arc (red band), and the Late Permian-Triassic
1319 arc built along the Cordilleran margin (orange band). Results from sample 383-2 are not
1320 included in this plot because of its uncertain stratigraphic position. Data from sample 131-2 are
1321 omitted because they differ from ages present in other samples from the Petrified Forest
1322 Member. Percent of all grains that are <240 Ma in age are shown for each sample on the left.

1323 **Figure 9.** MDS plot comparing age distributions of samples analyzed herein with each other and
1324 with possible source areas. MDS (metric) analyses are based on the cross-correlation
1325 coefficient, and were conducted using the software of Saylor et al. (2018). Data from samples
1326 analyzed herein are in DR Table 3. Ages for source regions are from the sources cited in the
1327 text. ~~Stars represent MDS values for sets of examples. Samples 383-2 with the exception that~~
1328 ~~sample 131 is not included with other Petrified Forest samples.~~ Stars represent MDS values for
1329 sets of examples, with the exception that sample 131 is not included with other Petrified Forest
1330 samples."

1331 **Figure 10.** Density distributions of U concentration versus U/Th for Triassic grains in the four
1332 chronostratigraphic units recognized in this study. Plots made with Hf density plotter software
1333 of Sundell et al. (2019).

1334 **Figure 11.** MDS plot comparing age distributions of Permian strata of the Colorado Plateau with
1335 each other and with potential source regions including the Appalachian orogen, Ouachita
1336 orogen, and basement rocks of southwestern North America. Data sources are described in
1337 Figures 3 and 4. The data support the interpretation of Lawton et al. (2015) that the Coconino,
1338 Cedar Mesa, and White Rim sandstones (cool shades) belong to a regional blanket of eolian

1339 strata that was derived largely from the Appalachian and/or Ouachita orogen, where strata of
1340 the Castle Valley and Cutler formations (warm shades) include greater proportions of detritus
1341 derived from local basement sources.

1342 **Figure 12.** Sketch map of relevant tectonic features in southwestern Laurentia during Late
1343 Triassic time [adapted from Figure 42 of Dickinson (2018)].

1344 **Figure 13.** Plot showing interpreted maximum depositional ages (and 2σ uncertainties) for each
1345 sample, as determined by the four methods described above and reported in DR Table 6.
1346 Preferred ages (vertical red lines) are the average of the ages calculated by these four methods.
1347 CA-TIMS and ID-TIMS ages are shown in approximate stratigraphic position (as shown by Kent
1348 et al., 2019), with outcrop samples in gray symbols and core samples using black symbols.
1349 Smaller symbols represent ID-TIMS ages or CA-TIMS ages based on a single age or of uncertain
1350 reliability. Stratigraphic units are keyed to dominant rock type, with brown = mudstone and
1351 siltstone, yellow = sandstone, pink = bentonite. Average grain size of each sample is shown with
1352 bars on left (from Appendix 1 and DR Table 1). PDP curves to right show 2.0 Ga to 240 Ma ages,
1353 as plotted on Figure 7. Also shown are age models of Kent et al. (2019) and Rasmussen et al.
1354 (2019). Vertical red bands show interpreted ages of main clusters of maximum depositional
1355 ages.

1356 Curves across top of diagram show the distribution of ages from (1) fore-arc strata of the
1357 Barranca and El Antimonio Groups in Sonora (Gonzalez-Leon et al., 2009; Gehrels and Pecha,
1358 2014) and the Great Valley Group in California (DeGraaff-Surpless et al., 2002; Surpless et al.,
1359 2006; Wright and Wyld, 2007), (2) Permian-Triassic igneous rocks in California (Chen and
1360 Moore, 2002; Miller et al., 1995; Tobisch et al., 2000; Barth and Wooden, 2006, 2011, 2013;
1361 Saleeby and Dunne, 2015), and (3) strata of the Chinle Formation in other parts of the Colorado
1362 Plateau (Dickinson and Gehrels, 2008; Riggs et al., 2012; Marsh et al., 2019). Diamond-shaped
1363 symbols beneath curves represent individual ages.

1364 **Figure 14.** Depositional model of strata of the Chinle Formation encountered in the CPCP core.
1365 Each time slice contains information about the dominant grain size of the host sedimentary
1366 rock, the abundance of syn-depositional-age zircon grains that are interpreted to be air-fall in
1367 origin, and the abundance of recycled zircon grains that pre-date deposition.